

# 冷原子中的凝聚态问题

(

<http://www.iphy.ac.cn>

Email: wmliu@aphy.iphy.ac.cn

Phone: 10-82649249(0)

# **Outline**

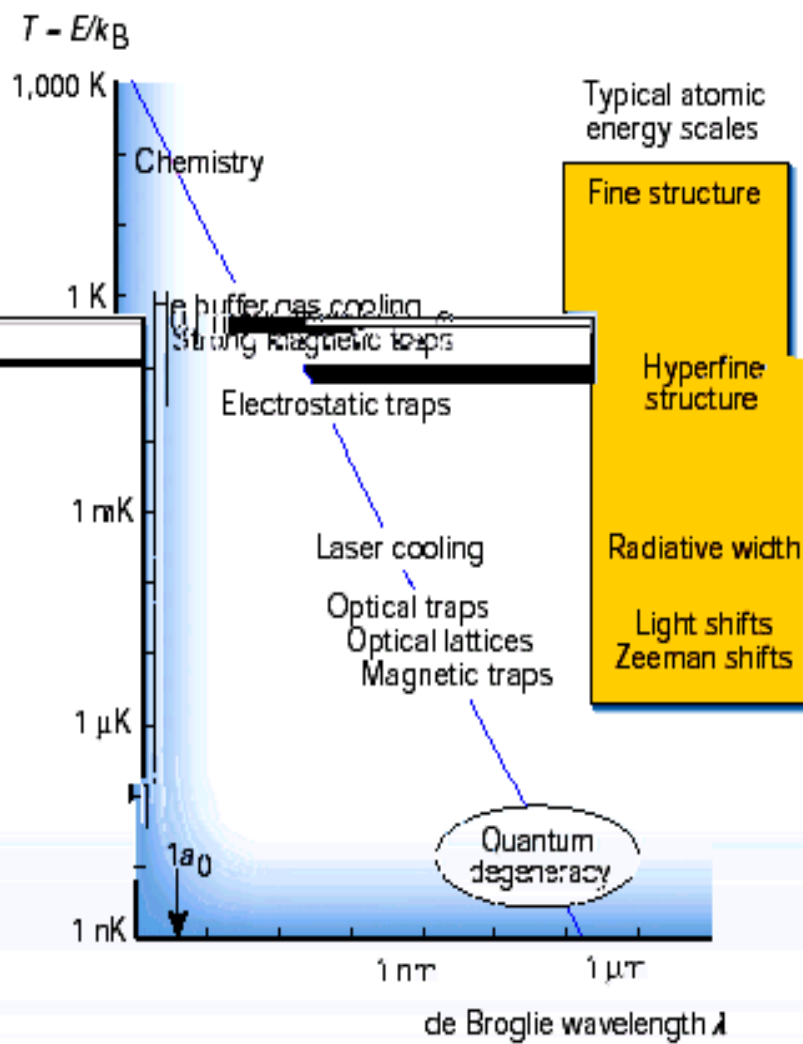
- 1. Introduction**
- 2. Superfluidity**
- 3. Quantum phase transition**
- 4. Strong correlated system**
- 5. Spinor BEC**
- 6. Boson - Fermion mixture**
- 7. BEC – BCS crossover**
- 8. Spin polarized fermi gas**
- 9. BEC in solid**
- 10. Application**
- 11. Outlook**

# 1. Introduction

**Figure 1** Overview of neutral atomic and molecular cooling and trapping. The energy scale spans 12 orders of magnitude in kinetic energy  $E$  of atomic motion, expressed in temperature units  $T = E/k_B$  ( $k_B$  is the Boltzmann constant). The length scale shows the corresponding de Broglie wavelength  $\lambda = h/p$  ( $h$  is the Planck constant), where momentum  $p = (2mE)^{1/2}$ . The line to guide the eye is calculated using the mass of the  $^{23}\text{Na}$  atom for  $m$ . Typical atomic dimensions are on the order of  $1a_0 = 0.0529\text{ nm}$ , the Bohr radius of the H atom, whereas Bose–Einstein condensates can have dimensions on the order of  $100\text{ }\mu\text{m}$ . The figure also indicates typical orders of magnitude for familiar energy scales associated with atomic fine structure, hyperfine structure, optical radiative broadenings, and optical or magnetic energy shifts. Cooling

requires a dissipative process to remove kinetic energy, whereas trapping requires a spatially dependent force to act on the atoms. Laser cooling<sup>2,4</sup> typically reaches kinetic energies below  $1\text{ mK}$ , where  $k_B T$  is smaller than natural line widths<sup>5</sup>, and atoms can be confined in a magneto-optical trap or optical trap. The latter uses a spatially dependent light shift attributable to a laser field to create a trapping potential for atoms. Similarly, a standing-wave light field can produce a periodic potential in space called an optical lattice<sup>6,7</sup>, with individual lattice cells spaced by  $\lambda/2$ , where  $\lambda$  is the wavelength of the lasers that make the lattice. Atoms whose magnetic Zeeman shift decreases with decreasing field strength can be trapped in a region of space with a magnetic field minimum. Evaporative cooling<sup>8</sup> of trapped atoms can dramatically lower the temperature and reach the limit of quantum degeneracy, where the phase space density  $\rho$ , defined as the number of particles

per cubic thermal de Broglie wavelength, is of order unity. If the atoms are bosons, then Bose–Einstein condensation occurs when  $\rho$  reaches the critical value of 2.6 (ref. 6; and see review in this issue by Anglin and Ketterle, pages 211–218).



# 超导超流与相变

1913 H. K. Onnes

1962 Lev Davidovich Landau

1972 J. Bardeen, L. N. Cooper, J.R. Schrieffer BCS

1973 Ivar Giaever , Brian D. Josephson

1978 Pyotr Leonidovich Kapitsa II

1982 Kenneth G. Wilson

1987 K. Alexander Muller, J. Georg Bednorz

1996 D. D. Osheroff, D. M. Lee, R. C. Richardson

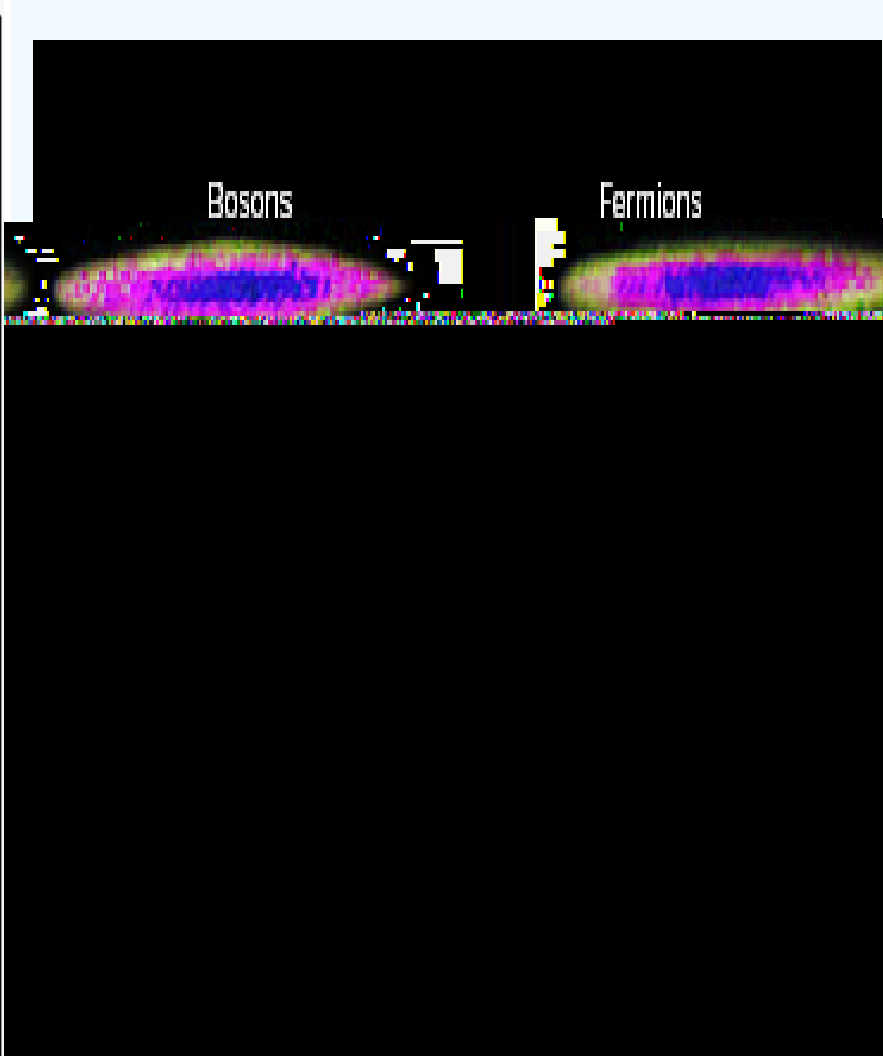
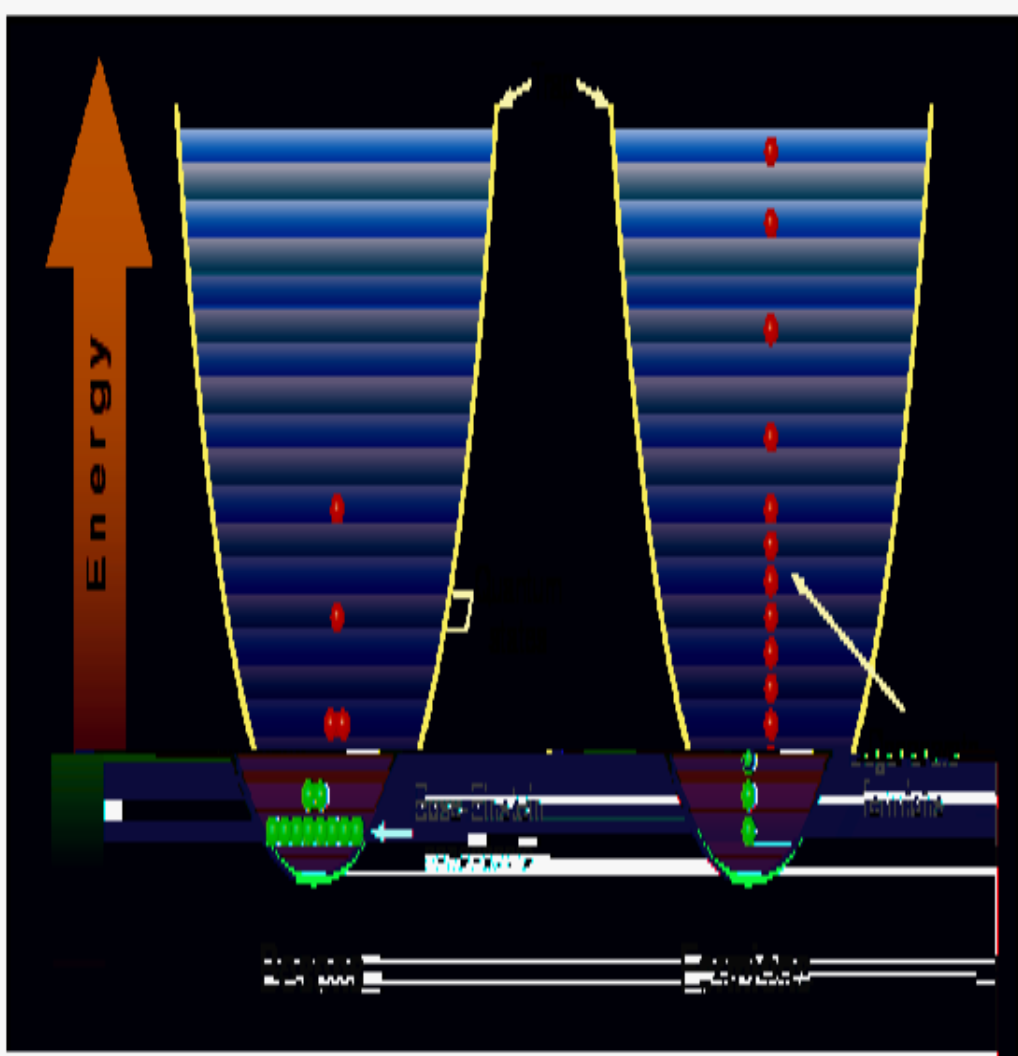
2001 E.A. Cornell, W. Ketterle, C.E. Wieman -

2003 A. A. Abrikosov, U. L. Ginzburg, A. J. Leggett

# 1.1. BEC of ideal gas

$^7\text{Li}$

$^6\text{Li}$



**spinons and ionomers.** Near absolute zero, identical bosons pile into the least energetic quantum state (left), whereas identical fermions stack into low-energy states one by one.

# 1.2. BEC in dilute gas

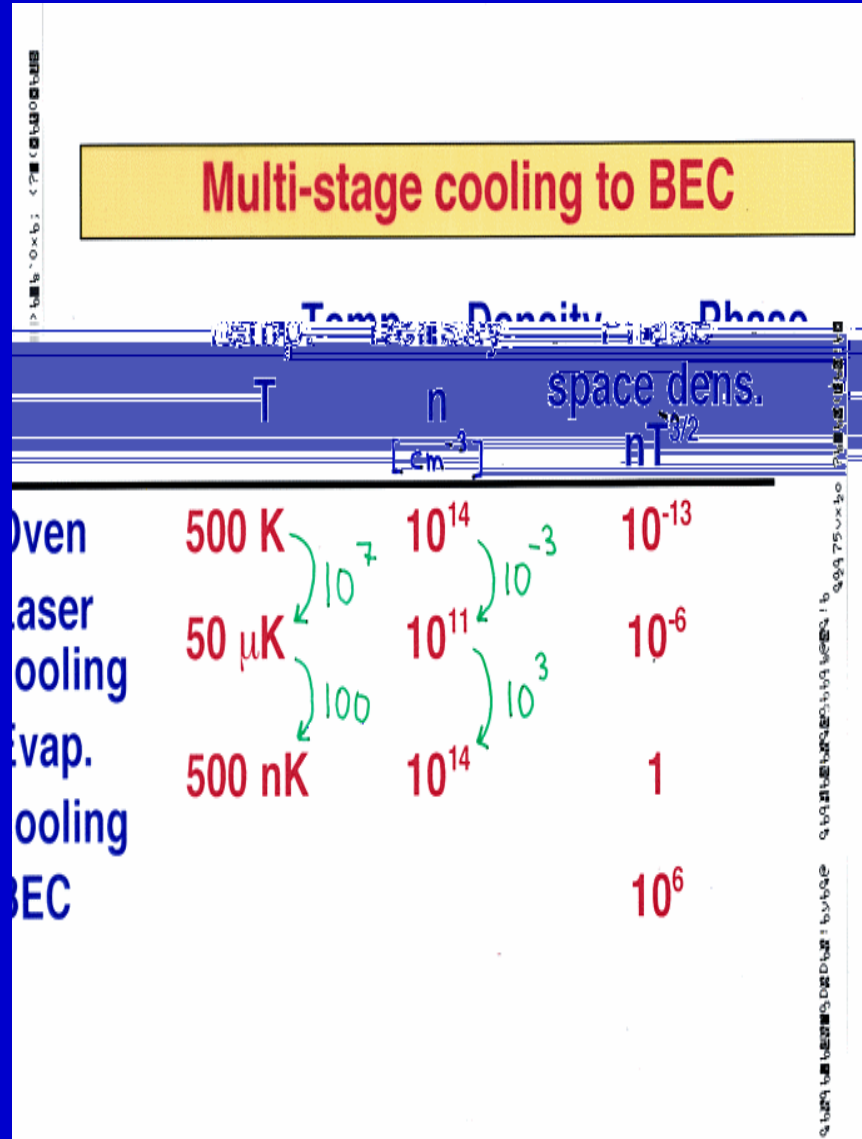
Laser cooling

Evaporative cooling—  
C.E. Wieman

Block—Rotating  
magnetic field—E.A.  
Cornell (Rb)

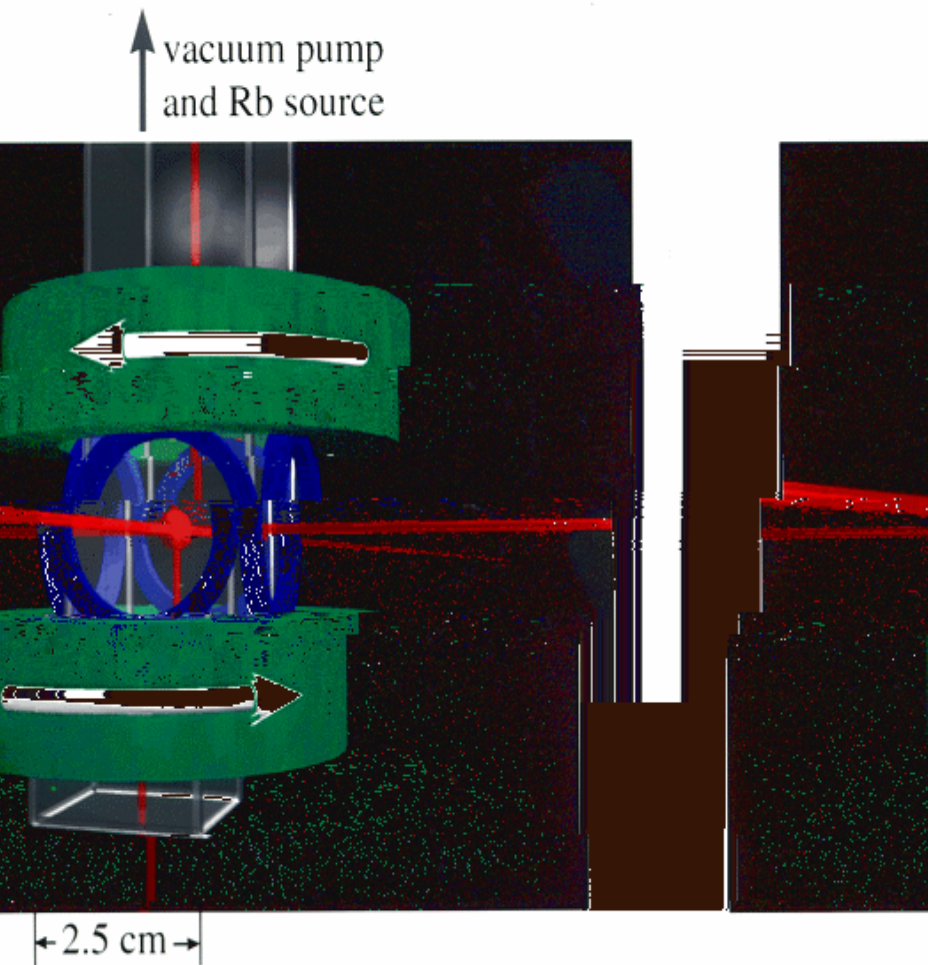
Block---laser beam—W.  
Ketterle (Na)

R. Hulet (Li) ???

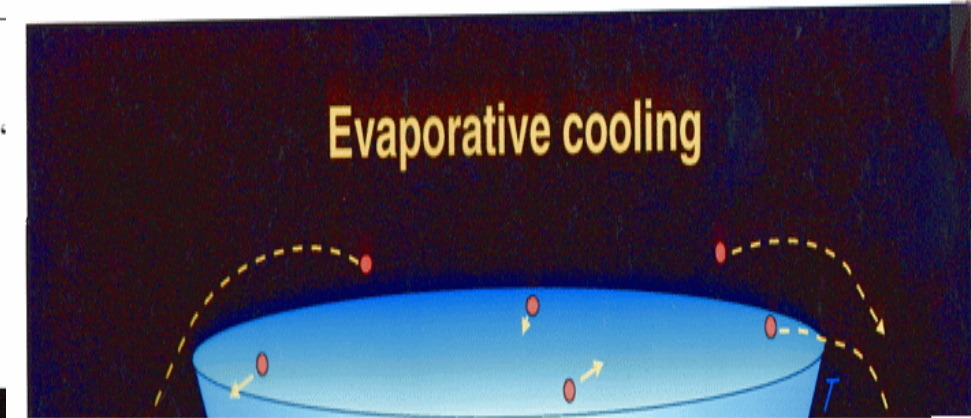


# EC Apparatus<sup>A</sup>

I" ~ 1/95- 11/96 (RIP Smithsonian)

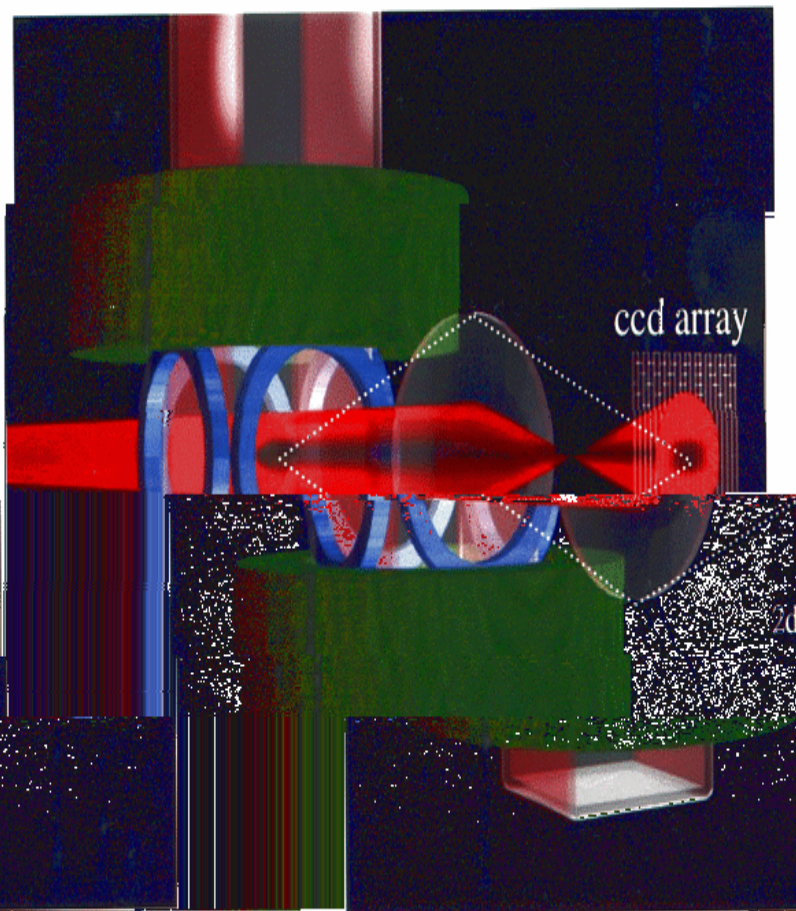


*Cheap diode lasers*



## Observing condensate

1. Expand cloud.
2. "Shadow snapshot".



Destroys condensate



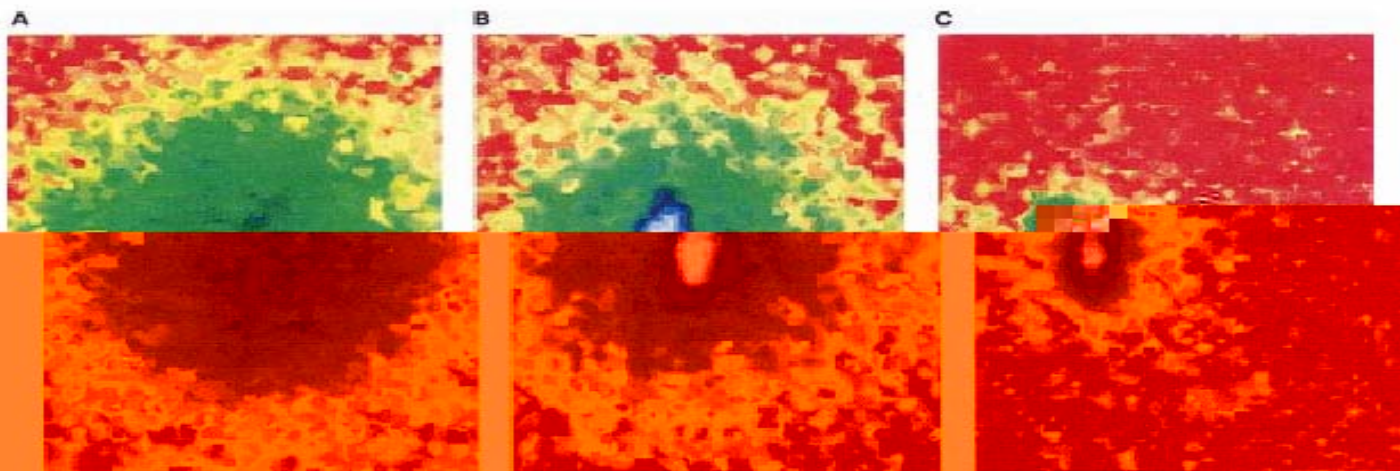
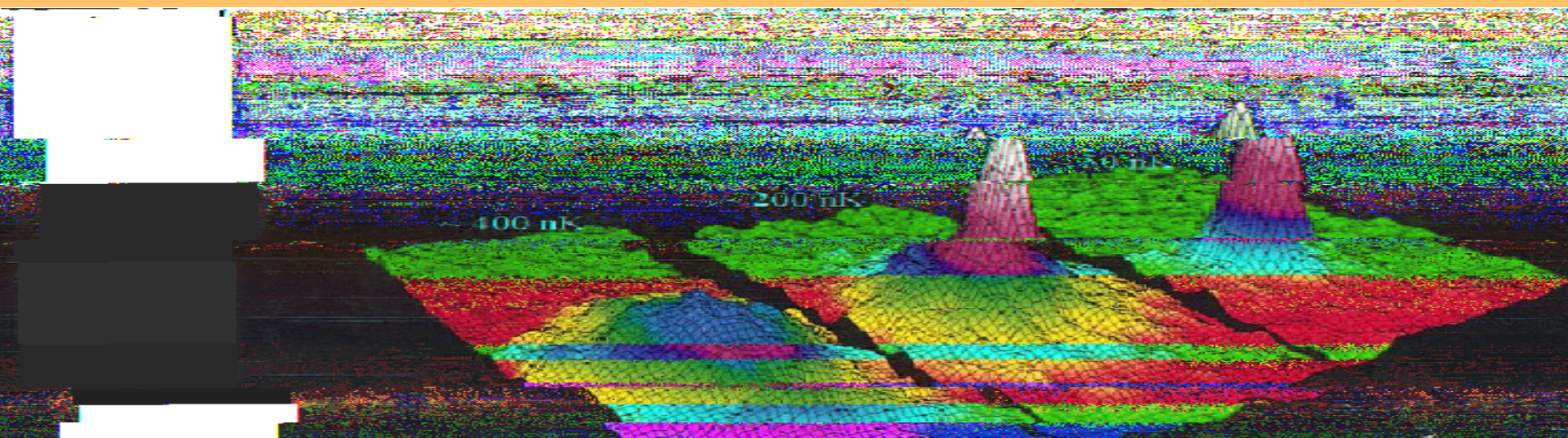


FIG. 8. Looking down on the three images of Figure 7 (Anderson *et al.*, 1995). The condensate in B and C is clearly elliptical in shape [Color].



PROTOTYPING  
AND DESIGN

WINTER TERM  
2018  
18.1.2018



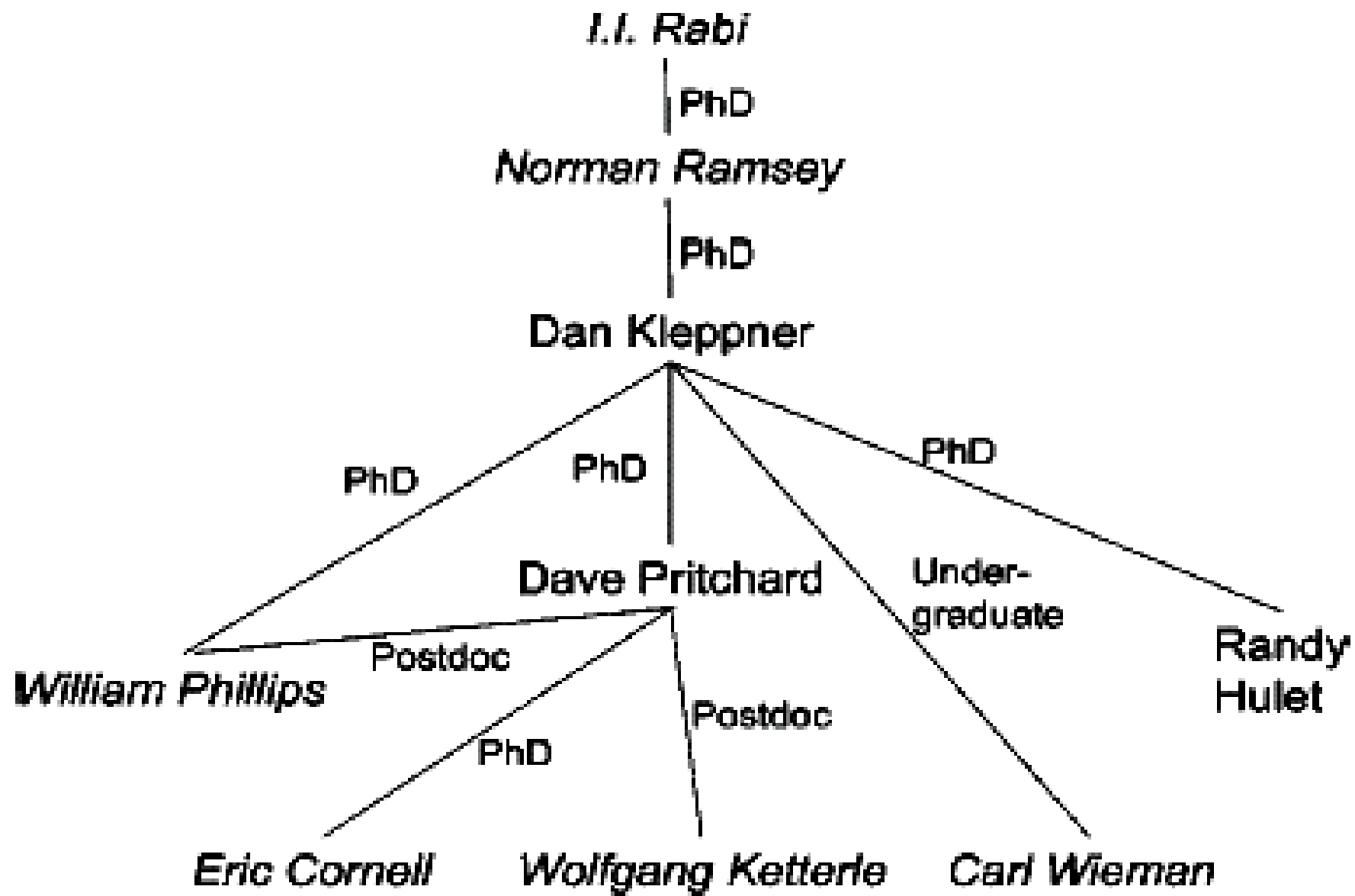
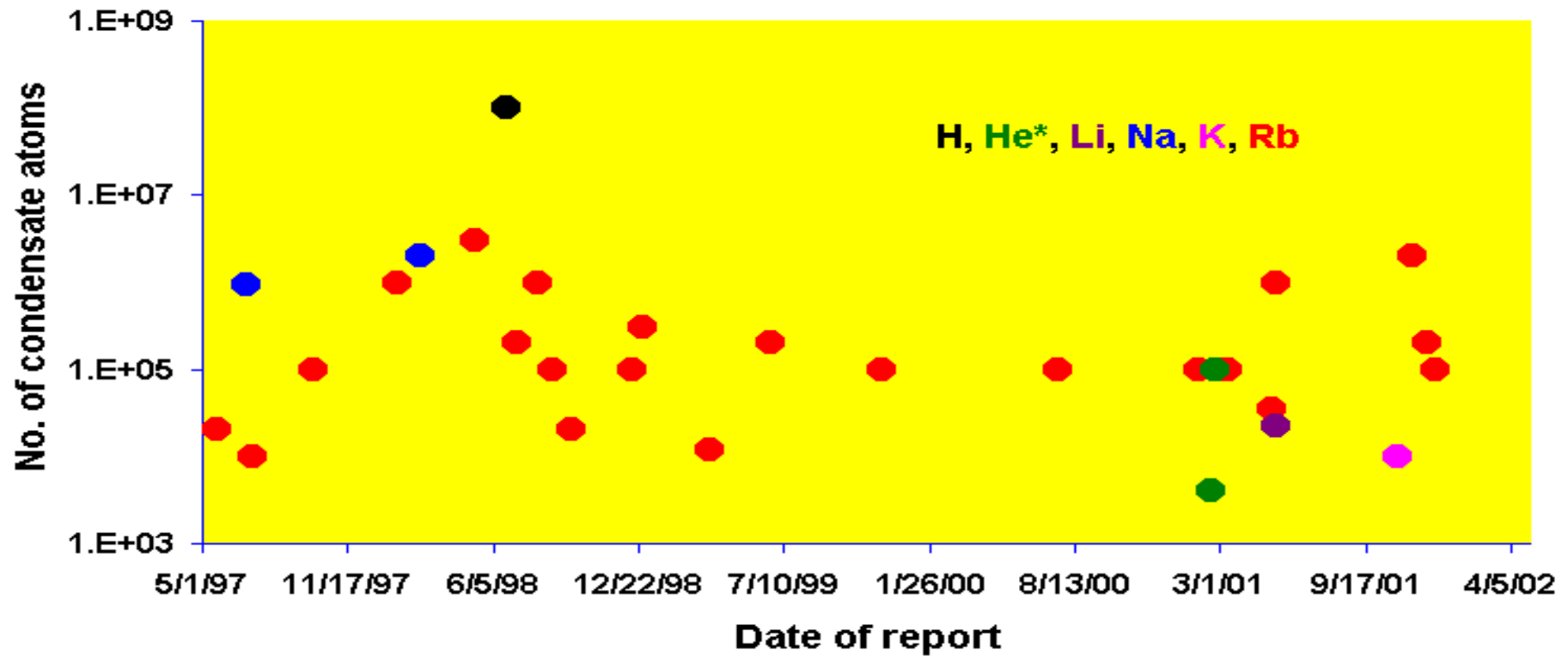


FIG. 10. Family tree of atomic physicists. People with names in italics are Nobel laureates.





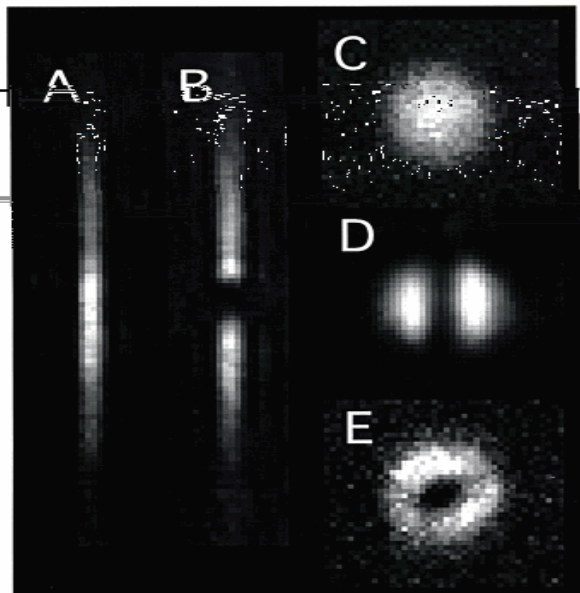
50 Lab.

- Elements: Li, Na, K, H, Rb, He, Fermi gases
  - Trapping techniques: **macroscopic chip** (Nature 413, 498 (2001))
  - Pure optics (Phys. Rev. Lett. 87, 010404 (2001))
  - Sympathetic cooling (Phys. Rev. Lett. 87, 080403 (2001))
  - Y.Z. Wang, Y.Q. Wang, BEC in China, March 2002, Shanghai, China**

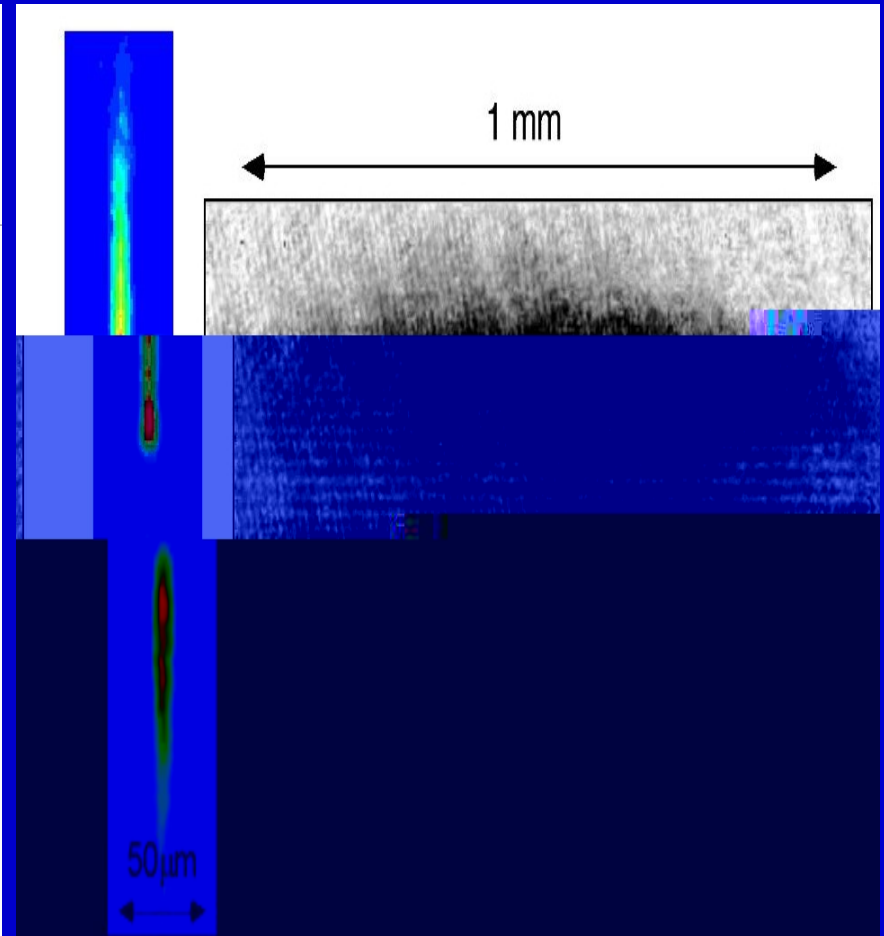
# 2. Superfluidity

## 2.1. Coherence

W. Ketterle, Science 275, 637 (1997).



Shaping condensates  
with magnetic fields and  
(far off-resonant) light





## The Nobel Prize in Physics 2001

◀ BACK ▶

To the left,  
Ketterle's first  
interference...  
pattern.

### Large condensates and interference patterns

Wolfgang Ketterle came to the Massachusetts Institute of Technology (MIT) in 1990. He worked with a different alkali atom, sodium, and published his BEC results four months after Cornell and Wieman, but with a condensate containing some hundreds of times more atoms. In an interference experiment he showed that all the atoms really were linked in a single wave of matter.

and then causing these to expand into each other, he could observe distinct interference patterns – rather like what happens when two stones are thrown into still water at the same time. The interference pattern would not have formed unless the matter waves were coherent.

ence pattern between two condensates resembles that of throwing two stones into still



The interference pattern formed by the expanding condensates.

– Atoms in unison | Particles or Waves? Both! | Cold... | ...colder... | ...coldest! | Large condensates and interference patterns | The atomic laser | Further reading | Credits |

Materials from the 2001 Nobel Poster for Physics

Version of the Nobel Poster from the Royal Swedish Academy of Sciences

**Contents:**  
| Introduction  
condensates and interference patterns | The atomic laser | Further reading | Credits |

Based on material from the 2001 Nobel Poster for Physics

Web Adapted by the Royal Swedish Academy of Sciences

**W.M. Liu, B. Wu, Q. Niu,**

**Nonlinear effects in interference  
of Bose-Einstein condensates,**

**Phys. Rev. Lett. 84, 2294 (2000).**

**SCI 121**

# Many-body Hamiltonian

$$H = \frac{1}{2} \int dr \left[ \frac{\hbar^2}{2m} \nabla^2 + V_{ext}(r) \right] \psi(r)^* \psi(r)$$

The mean field theory

$$\psi(r,t) \sim \psi_0(r,t)$$

Gross-Pitaevskii equation

$$i\hbar \frac{\partial}{\partial t} \psi_0(r,t) = -\frac{\hbar^2}{2m} \nabla^2 \psi_0(r,t) + V_{ext}(r,t) \psi_0(r,t)$$

# Gross-Pitaevskii equation

$$i\hbar \frac{\partial}{t} - \frac{\hbar^2 \nabla^2}{2m} - V_{ext}(r) - \frac{4\pi \hbar^2 a}{m} | \psi |^2$$

## Long time solution

$$(x, t) = \frac{(\frac{x}{t})}{\sqrt{t}} e^{i \frac{x^2}{2t} - i 2 \left| (\frac{x}{t}) \right|^2 \log(4t)} + O(t^{-1} \log t)$$

$$| \psi(k) |^2 = \frac{1}{2g} \log(1 - | r(k) |^2)$$

# Theoretical explanation

## Fringe position

$$k_n = \frac{2\sqrt{E_n}}{2 V_0} = n - \frac{1}{2} \sqrt{2V_0}^{1/2}$$

## Central fringe

$$k_0 = k_1 = k_{11} = 4 V_0 \sqrt{V_0/2}^{1/2}$$

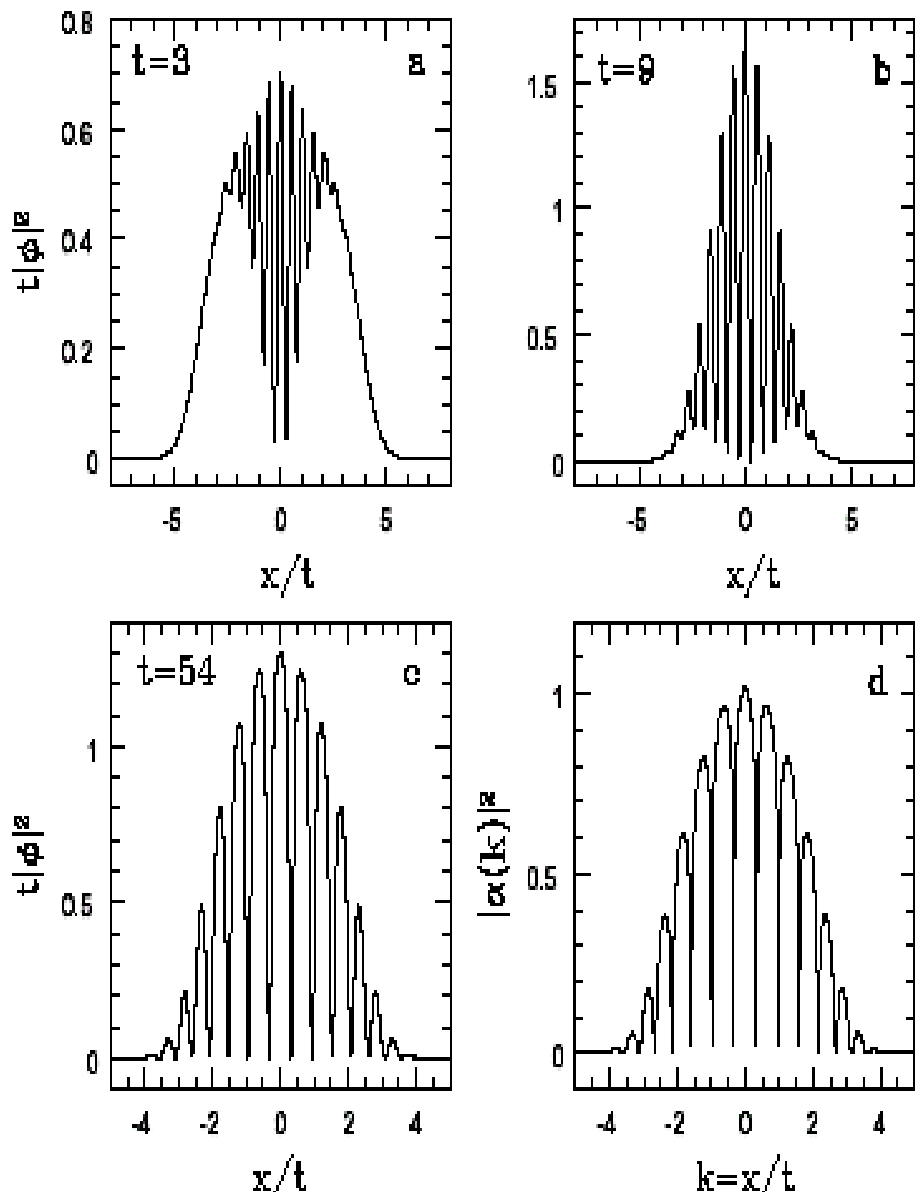


FIG. 1. Evolution of two BECs ( $g = 2, d_0 = 12, \sigma = 1$ ). The scaled packets at (a)  $t = 3$ , (b)  $t = 9$ , and (c)  $t = 54$ . (d)  $|\alpha(k)|^2$  in Eq. (4).

# Experimental prediction:

1. Energy level
2. Many wave packets

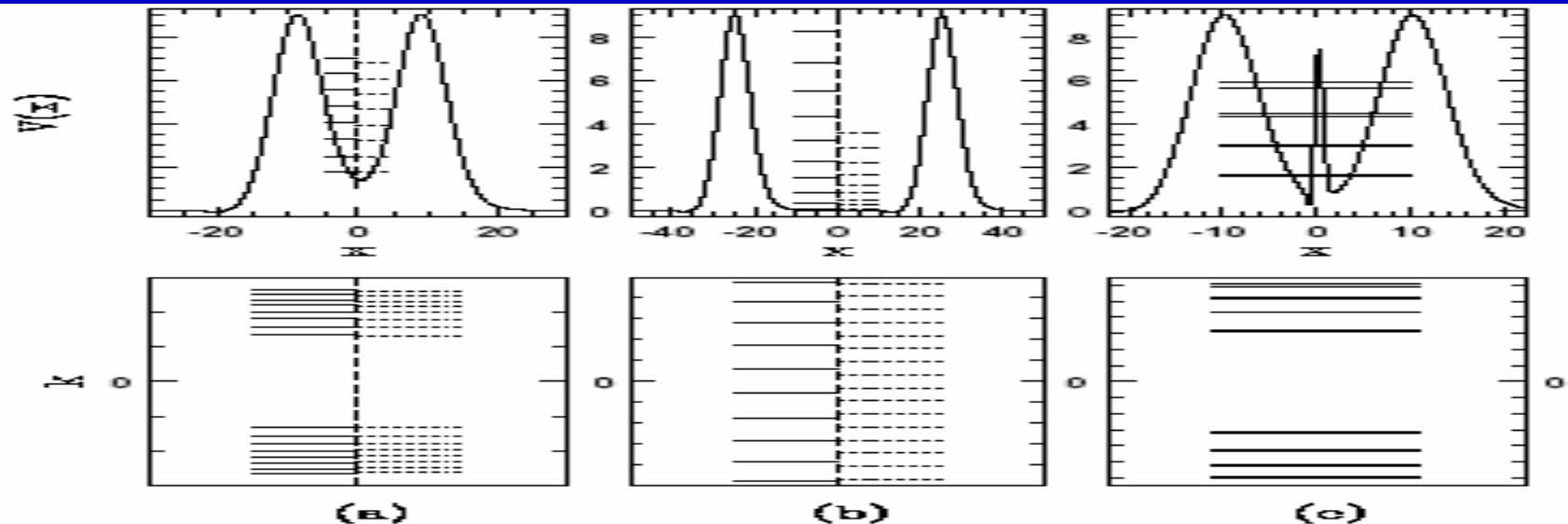


FIG. 2. The potentials, the energy levels, and the levels in  $k$ . Two Gaussian wave packets with (a) small separation, (b) large separation, and (c) three Gaussian wave packets. The solid level lines are accurate numerical results while the dotted lines are analytical results for comparison. Note that the energy levels in (b) are magnified by a factor of 10; the  $k$  level spacing is the same as spacing for the reference model in the main text.

## Ratio of level width to level spacing

$$\frac{k_n}{k_n} = \frac{E_n}{E_n} = 2e^{-2\sqrt{g-E_n}w} = E_n$$

**W.D. Li, X.J. Zhou, Y.Q. Wang, J.Q. Liang, W.M. Liu,**

**Time evolution of relative phase  
in two-component Bose-Einstein  
condensates with a coupling drive,**

**Phys. Rev. A64, 015602 (2001).**

## 2.2. Josephson effect

M.A. Kasevich, Science 298, 1363 (2002).

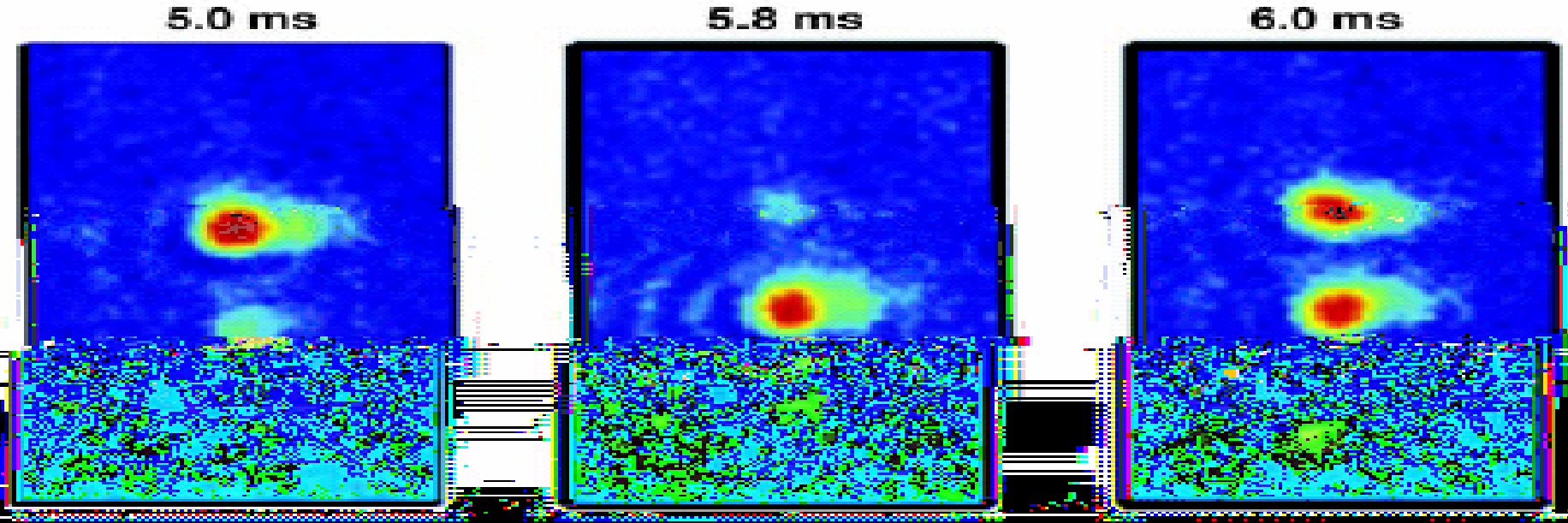


Fig. 6. AC Josephson effect in optical lattices, as observed through the interference profile of atoms suddenly released from a vertically rotating cold atom interferometer optical lattice. The relative phase  $\phi$  between adjacent wells evolves according to the Josephson relation  $\phi(t) = \frac{2\pi}{\hbar} \frac{\partial E}{\partial \phi} t + \phi_0$ , where  $\hbar$  is Planck's constant,  $t$  is time, and  $\phi_0$  is the chemical potential difference between adjacent wells. This evolution results in an oscillation of the populations of diffraction lobes in the interference signals. In this work,  $\phi$  is determined by gravity. The time label references the time interval that the atoms were held in the counterfactual groundstate plus about 100 ms to account for the readout process.

# Quantum tunneling

W.M. Liu, W.B. Fan, W.M. Zheng, J.Q. Liang, S.T. Chui,

Quantum tunneling of  
Bose-Einstein condensates  
in optical lattices under gravity,

Phys. Rev. Lett. 88, 170408 (2002).

SCI

92

# Potential energy and Bloch bands

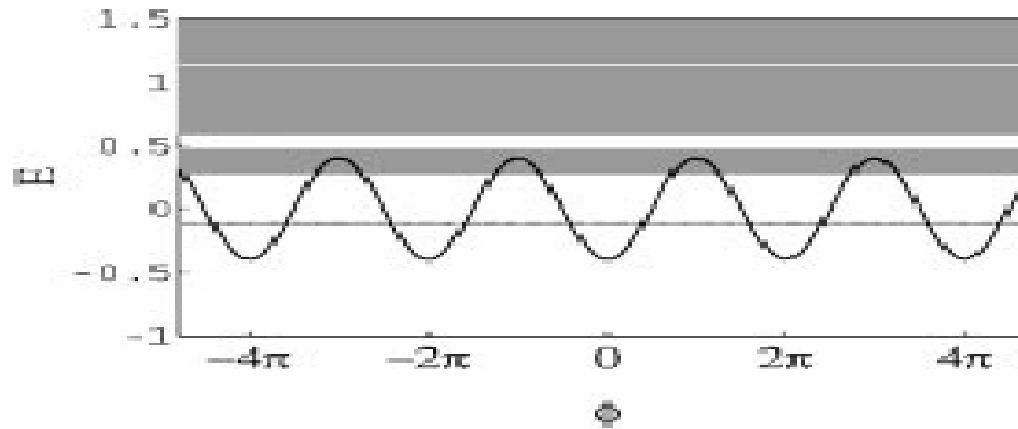


FIG. 1. Potential energy  $V_0 \cos\phi$  and the Bloch bands for  $V_0 = 0.4$ .

## Landau-Zener tunneling

- Barrier between lattices is low
- Localized level between lattices is coupling
- Miniband
- Adiabatic approximation
- Tunneling between delocalized states in different Bloch bands

# Tilted bands and WS ladders

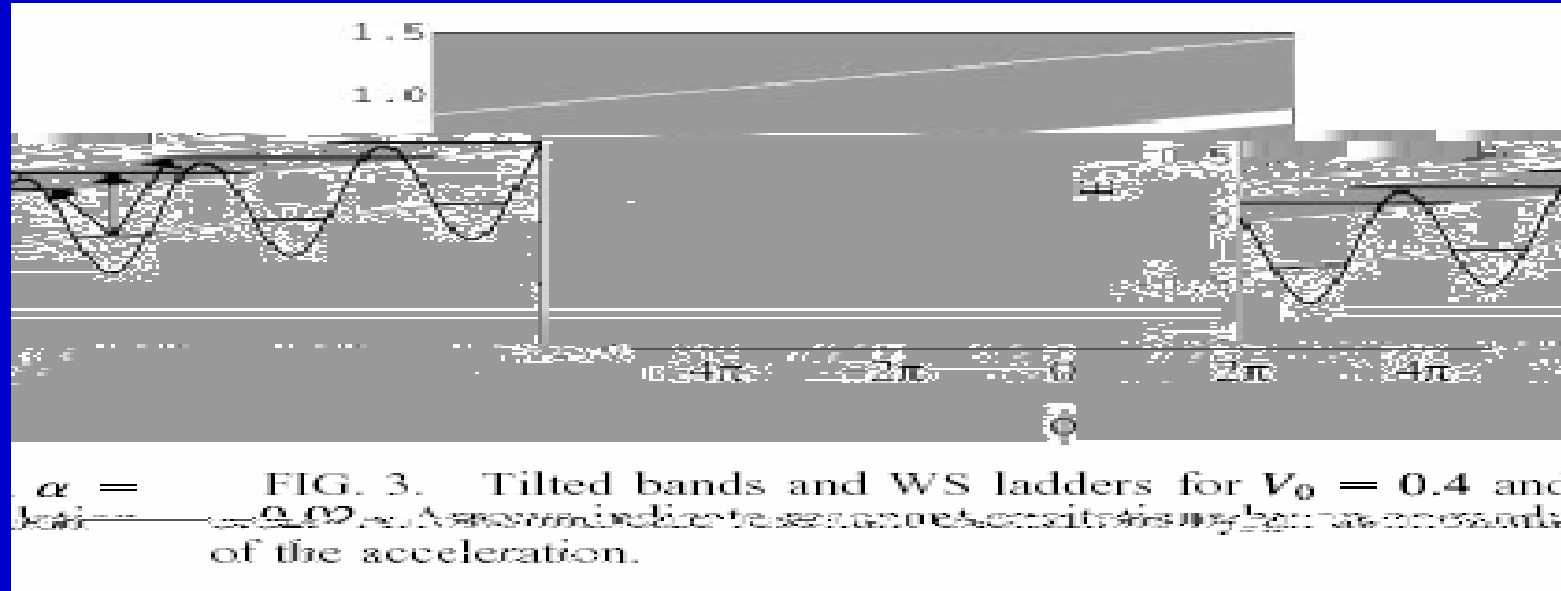


FIG. 3. Tilted bands and WS ladders for  $V_0 = 0.4$  and  $\omega = 0.02$ . The parameter  $\alpha$  determines the number of minima of the acceleration.

## Wannier-Stark tunneling

- An external field
- Wavefunction of miniband is localization
- Miniband is divided into discrete level
- Wannier-Stark ladder
- Tunneling between localized states in different individual wells—Wannier-Stark localized states

# Temperature dependence

$$(T) = \frac{\hbar w_0}{k_B T} \left( 1 - e^{-\frac{\hbar w_0}{k_B T}} \right) e^{\frac{432 V_{\max}}{\hbar w_0} e^{\frac{\hbar w_0}{k_B T}}}$$

At high temperature:  
Arrhenius law

$$AR = \frac{0}{2} e^{-V_{\max}/k_B T}$$

At intermediate temperature:  
Thermally assisted tunneling

$$T_{cr} \quad \frac{hw_0}{2 k_B}$$

Crossover temperature

$$T_{cr} \quad 257nK$$

$$U_l(x, y) \quad 2.1E_R$$

At low temperature:  
Pure quantum tunneling

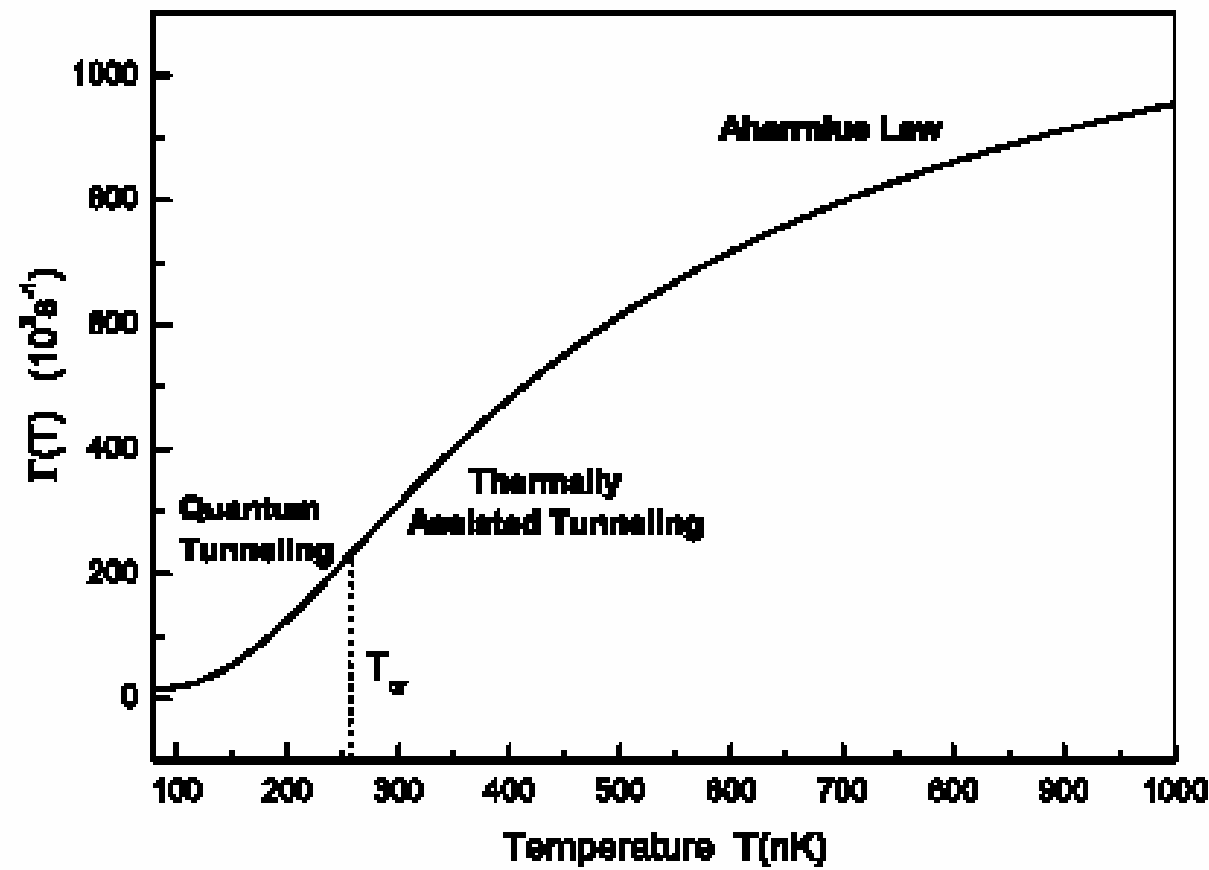
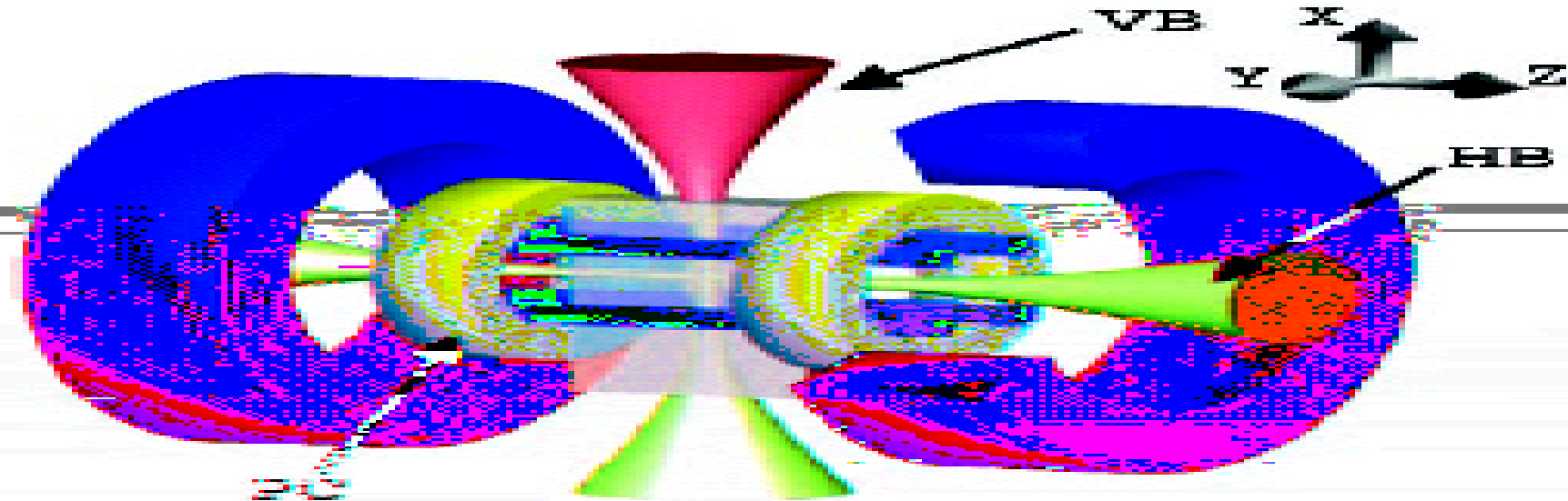


FIG. 1. The temperature dependence of the decay rate  $\Gamma(T)$  for  $^{87}\text{Rb}$  atoms with Yale experimental parameters  $\lambda = 850 \text{ nm}$ ,  $U_l(x, y) = 2.1E_R$ , where  $E_R = \frac{2\pi^2\hbar^2}{m\lambda^2}$  is the recoil energy.

## 2.3. Soliton

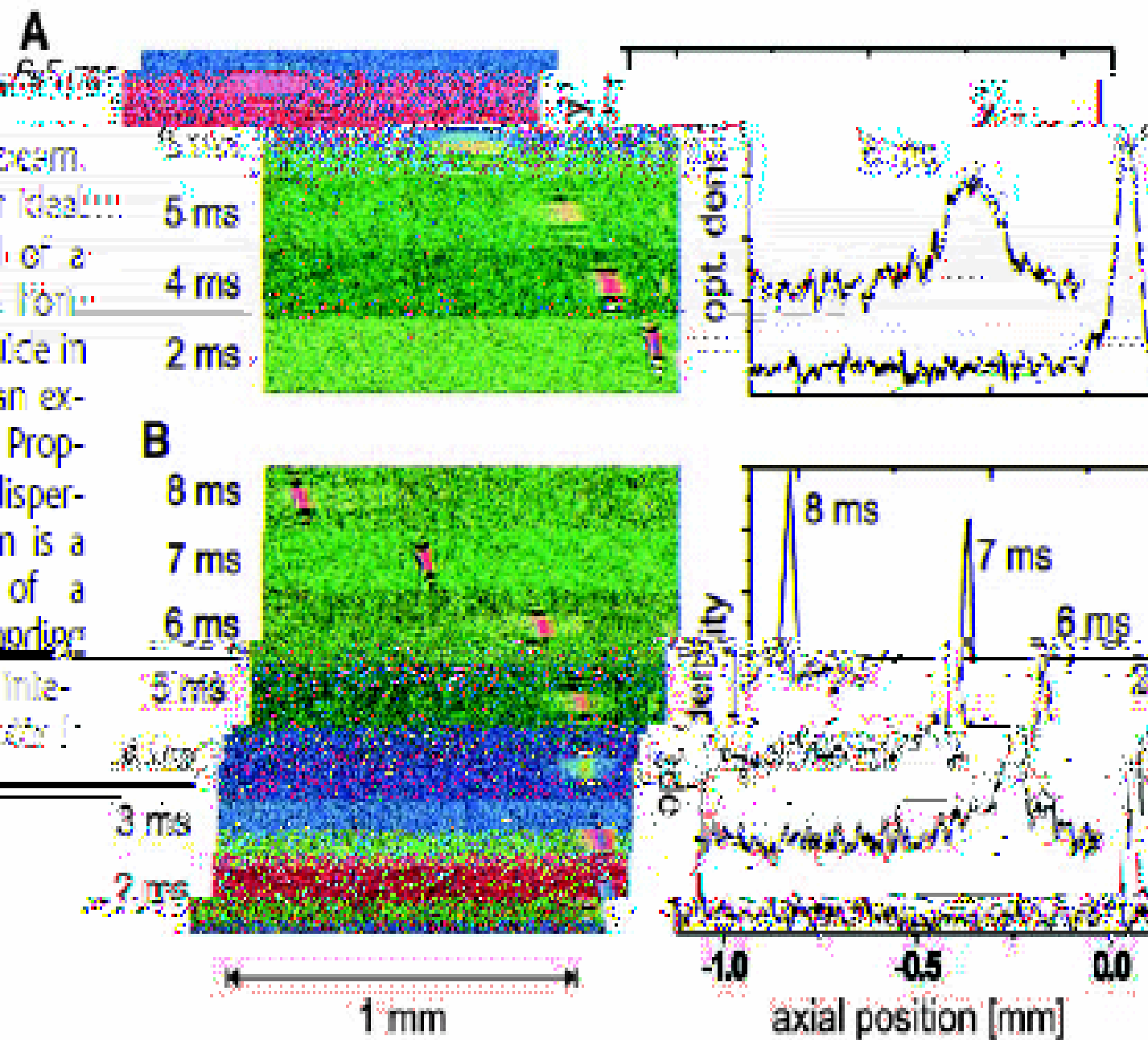
L. Khaykovich et al., Science 296, 1290 (2002).



**Fig. 1.** Experimental setup for soliton production.  $^{7}\text{Li}$  atoms are evaporatively cooled in a Ioffe-Pritchard magnetic trap and transferred into a crossed optical dipole trap in state  $|F = 1, m_F = 1\rangle$  where they Bose condense. Magnetic tuning of the scattering length to positive, zero, and negative values is performed with the two pinch coils (PC). Switching-off the vertical trapping beam (VB) allows propagation of a soliton in the transversal 1D waveguide (HB). Atom detection is done with a CCD camera in reconded on a charge-coupled device camera in the x, z plane.

**Fig. 3.** Absorption images at variable delays after switching off the vertical trapping beam.

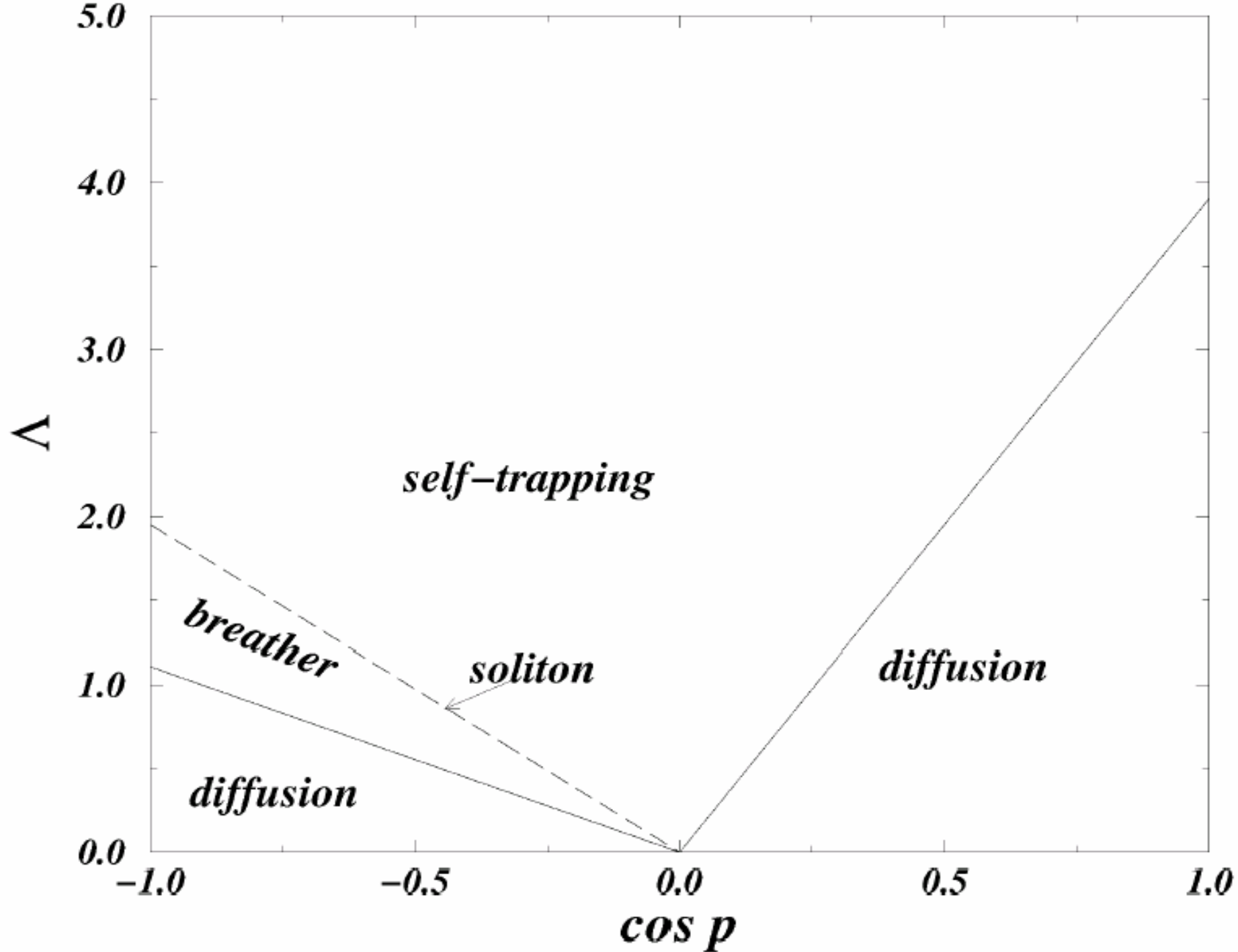
Propagation of an ideal 360° ges (A) and of a soliton (B) in the horizontal 1D waveguide in the presence of an expulsive potential. Propagation without dispersion over 1.1 mm is a clear signature of a soliton. Corresponding axial profiles are integrated along the direction:



Z.W. Xie, Z.X. Cao, E.I. Kats, W.M. Liu,

Nonlinear dynamics  
of dipolar Bose-Einstein condensate  
in optical lattice,

Phys. Rev. A 71, 025601 (2005).



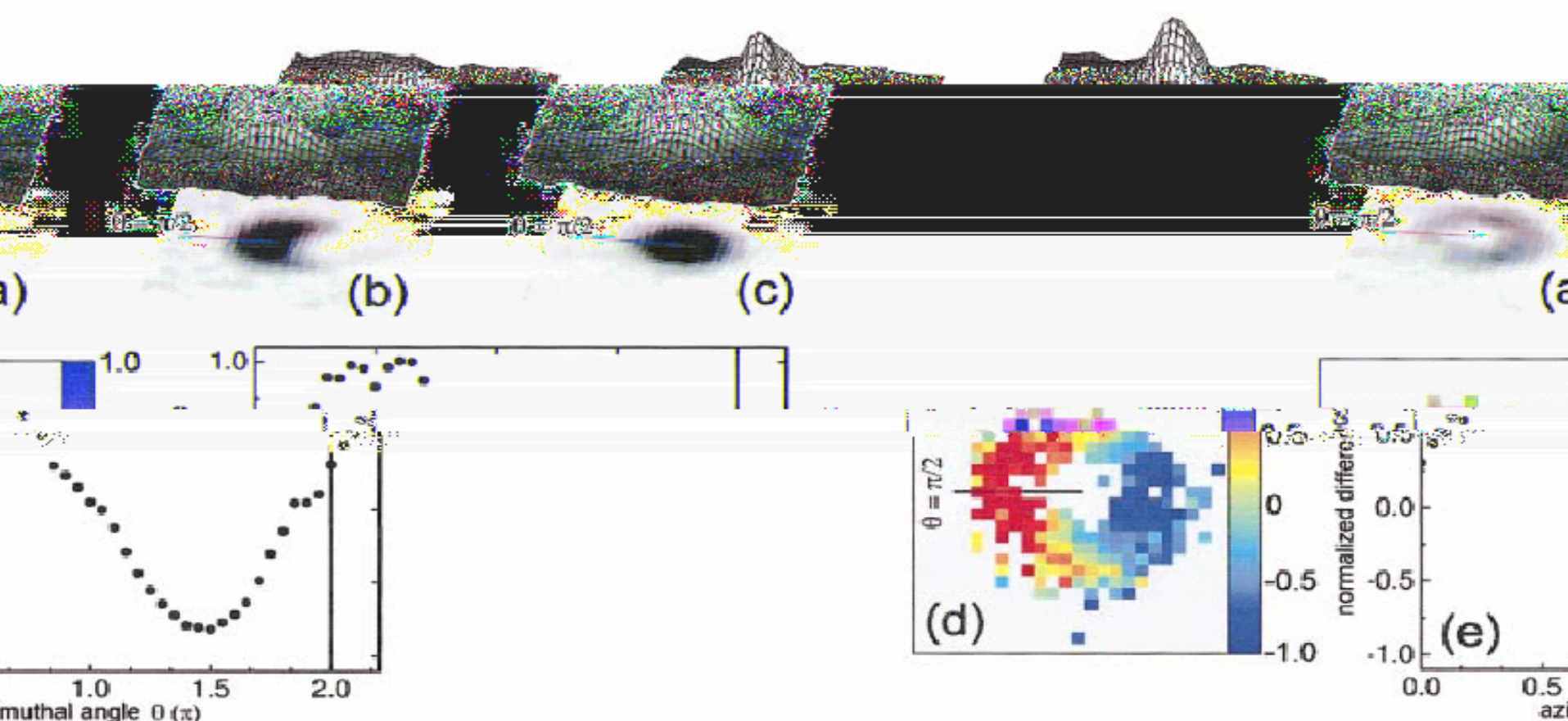
**L. Li, B.A. Malomed, D. Mihalache, W.M. Liu,**

**Exact soliton-on-plane-wave  
solutions for two-component  
Bose-Einstein condensates,**

**Phys. Rev. E 73, 066610 (2006).**

## 2.4. Vortex and Abrikosov lattices

J. R. Abo-Shaeer et al., Science 292, 476 (2001).



ement of its phase as a function of azimuthal angle: (a) ... FIG. 11. Condensate images showing the first BEC vortex and the measure-  
ments made below just in that state in a way that forms a vortex. The density distribution of atoms in the upper hyperbolic state after ad-  
dition of lower hyperbolic states for rings with angular momentum ... (b), the same state after a  $\pi/2$  pulse has been applied, that drives  
superfluidity and vortices to the lower hyperbolic state, in which the vortex ... collecting the phase distribution of the sys-  
tem shown in (b); (c) a color map of the phase differences measured in (b); (d) radial ... found that interface with  $\theta = \pi/2$  gives the in-  
tegral ... The data are repeated after the azimuthal angle  $2\pi$  to better show the continuity. averages at each angle ... around the rings in (c)  
and (d). This shows that clear and clean ring ... the other phases winding expected for a quasimomentum with a  
angular momentum. From Mattheson et al., 1999a [Color].

# Superfluidity

L. Pitaevskii et al., Science 298, 2144 (2002).

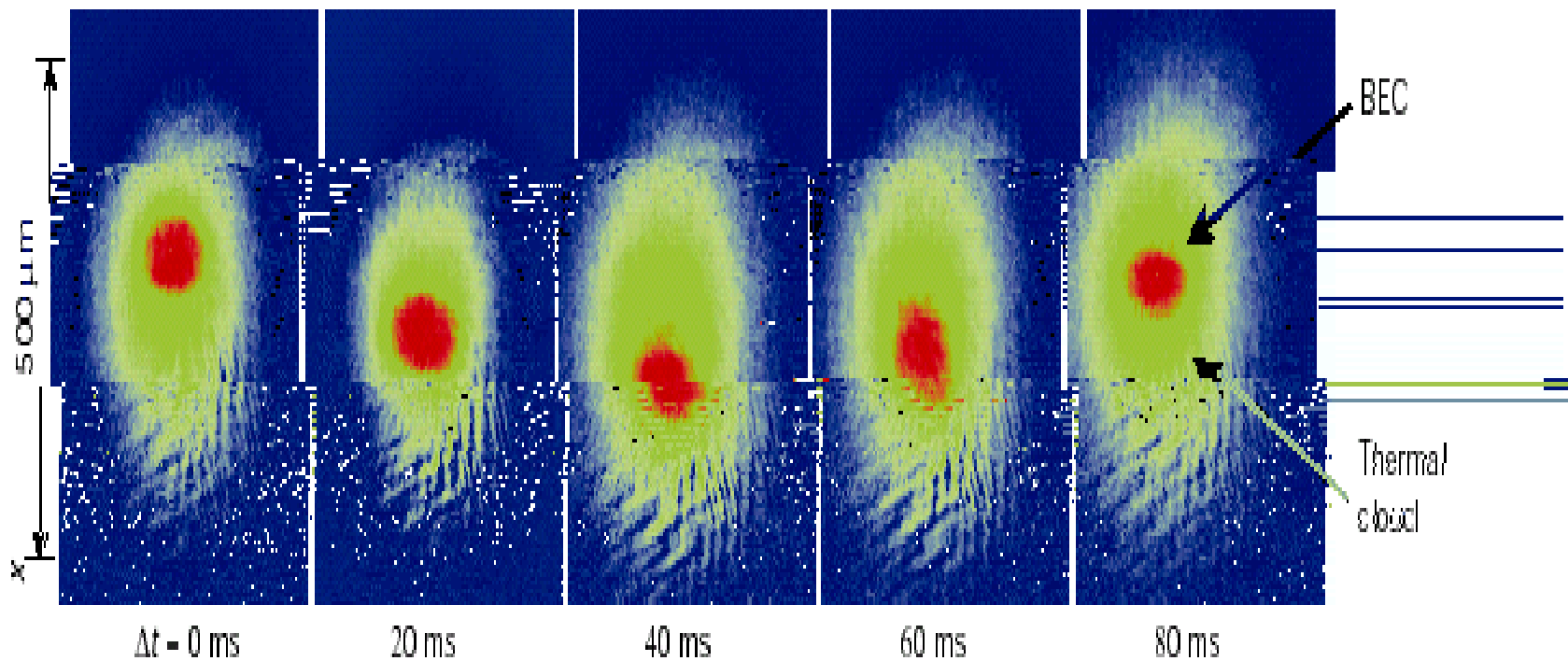


**Figure 4** Signature of superfluidity in a Bose-condensed cloud<sup>13</sup>. The condensate and its thermal ‘halo’ of normal gas respond differently when they are dragged through a periodic potential. In the experiment, the clouds were displaced in a magnetic trap superimposed by an optical lattice. The condensate, distinguished by its much higher

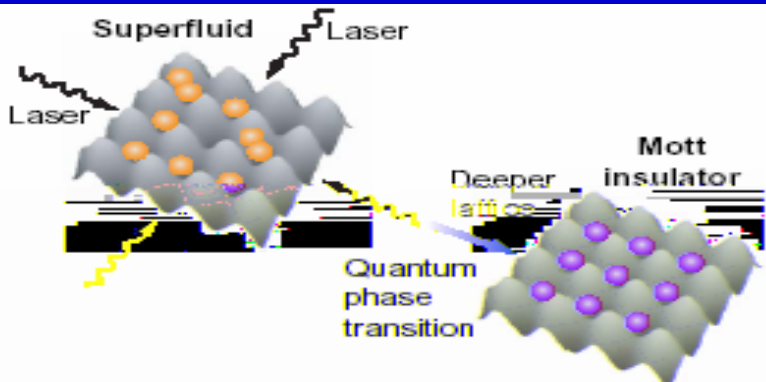
density (colour coded in red), tunnelled through the potential peaks and oscillated in the magnetic trapping potential, whereas the normal fraction was pinned by the optical lattice. Interaction between the two clouds eventually led to damping of the condensate motion.

# 3. Quantum phase transition

Superfluid  
Mott insulator

Insulator + disorder = Bose glass  
Insulator + weak disorder = Anderson glass

Berezinskii–Kosterlitz–Thouless transation



**Cold atoms in optical lattices.** (Top) Cold atoms in a periodic optical potential localize near the potential minima. The atoms can tunnel to neighboring sites with hopping amplitude  $J$ . Atoms on the same site repel each other according to the onsite interaction  $U$ . For weak lattices ( $J \gg U$ ), the atoms form a superfluid (BEC) with atoms delocalized over many lattice sites. With increasing laser intensity ( $J \ll U$ ), the atoms form a Mott insulator state in which atoms are locked at individual lattice sites (3). (Bottom) Experimental signatures of the superfluid–Mott insulator transition (4). In the superfluid (rear), the atoms show an interference pattern, which disappears in the Mott phase (front). (Right) Entangling atoms in a lattice. Depending on their internal state, atoms collide with neighboring atoms when the potential holding atoms in one state is moved while the potential holding atoms in the other state is kept stationary (11, 12).

J.J. Liang, J.Q. Liang, W.M. Liu,

Quantum phase transition  
of condensed bosons in optical lattices,

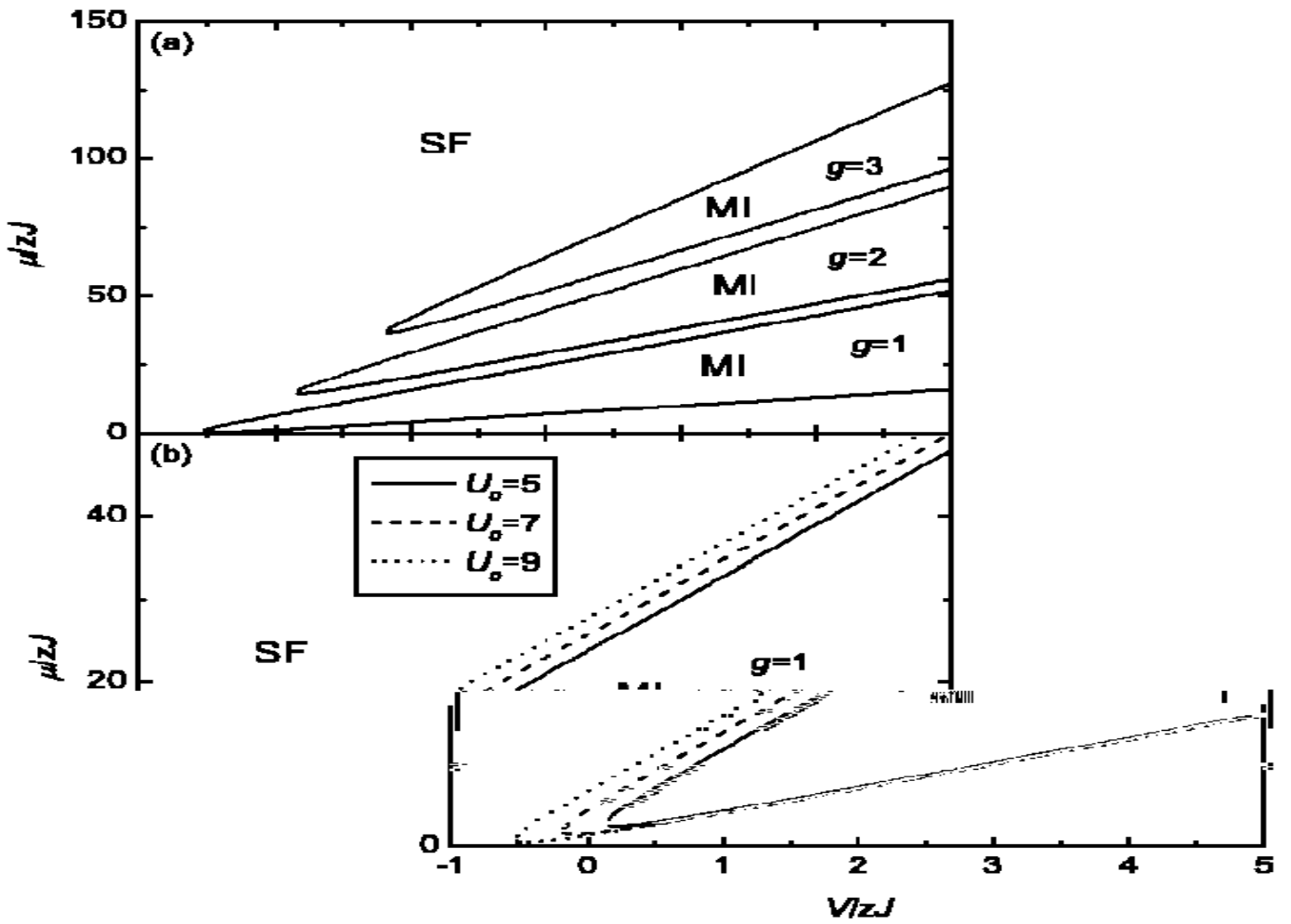
Phys. Rev. A68, 043605 (2003).

SCI 32

**Z.W. Xie, W.M. Liu,**

**Superfluid–Mott insulator transition  
of dipolar bosons in an optical lattice,**

**Phys. Rev. A70, 045602 (2004).**



model in an optical lattice with (a)  $U_0=9$  and (b) different on-site interactions  $U_0=5$ , 7. The vertical axis shows the dimensionless chemical potential  $\mu/\bar{z}J = \bar{\mu}/\bar{z}J$  and the horizontal axis shows the dimensionless dipole-dipole interaction  $V/zJ = \bar{V}$ . “SF” and “MI” mean “superfluid” and “Mott-insulator phase”, respectively.

G.P. Zheng, J.Q. Liang, W.M. Liu,

Phase diagram of  
**two-species** Bose-Einstein condensates  
in an optical lattice

Phys. Rev. A71, 053608 (2005)

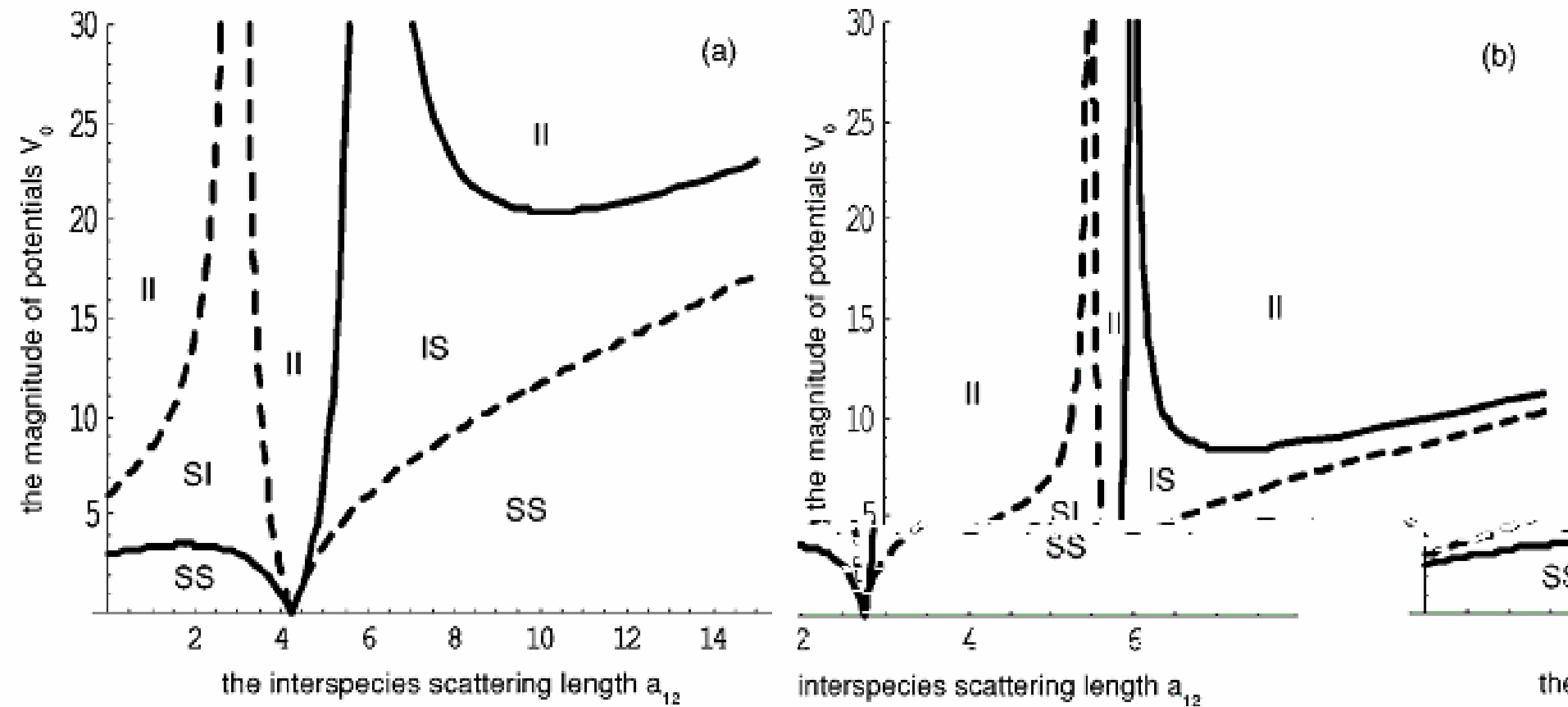


FIG. 1. Phase diagrams of two-species BECs in a 1D optical lattice. The magnitude of potentials  $V_0$  is in units of  $4n\hbar\omega_0$ . The interspecies scattering length is in units of nm. Dashed curves: phase boundary of species 1; solid curves: phase boundary of species 2. The  $s$ -wave scattering lengths between the same species are (a)  $a_1=6 \text{ nm}$  ( $^{87}\text{Rb}$ ),  $a_2=3 \text{ nm}$  ( $^{23}\text{Na}$ ). (b)  $a_1=3 \text{ nm}$  (hyperfine state  $|f=1, m_f=1\rangle$  of  $^{23}\text{Na}$ ),  $a_2=2.5 \text{ nm}$  (hyperfine state  $|f=1, m_f=0\rangle$  of  $^{23}\text{Na}$ ). The  $s$ -wave scattering lengths between different species are as follows: (a)  $a_{11}=10 \text{ nm}$  ( $^{87}\text{Rb}$ ),  $a_{22}=1 \text{ nm}$  ( $^{23}\text{Na}$ ); (b)  $a_{11}=1 \text{ nm}$  ( $^{23}\text{Na}$ ),  $a_{22}=0.5 \text{ nm}$  ( $^{87}\text{Rb}$ ).

P.B. He, Q. Sun, S.Q. Shen, W. M. Liu,

Magnetic quantum phase transition of  
cold atoms in optical lattice,

Phys. Rev. A 76, 043618 (2007).



A.C. Ji, X.C. Xie, W. M. Liu,

Magnetic dynamics of polarized light in  
arrays of microcavities,

Phys. Rev. Lett. 99, 183602 (2007).





## 4. Strong correlated system

4.1. Strong interacting system

4.2. Strong correlated system

4.3. Quantum Hall effect

# BEC near Feshbach resonance

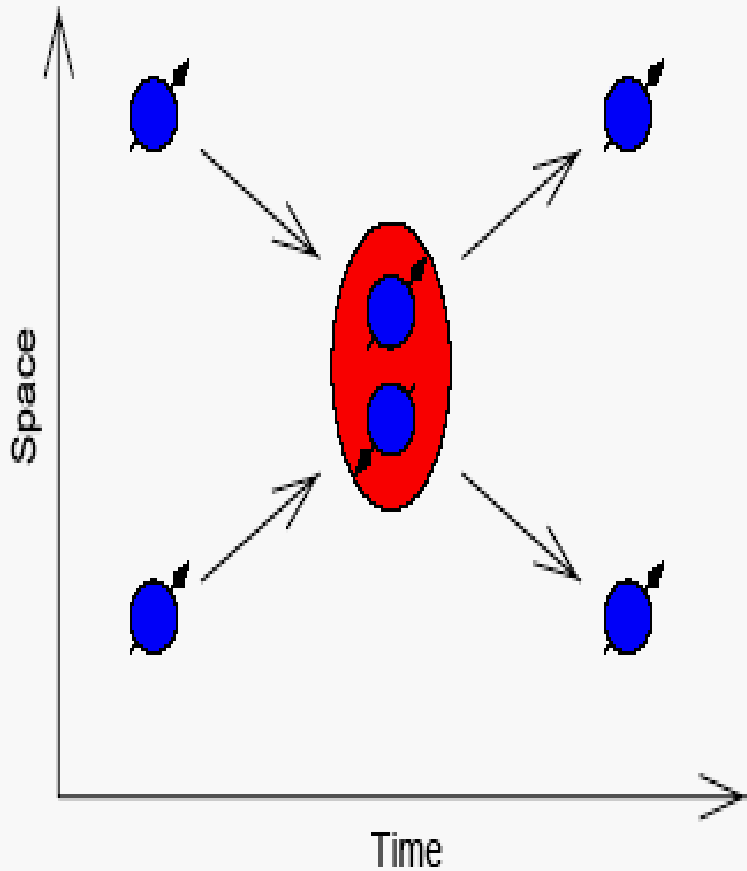
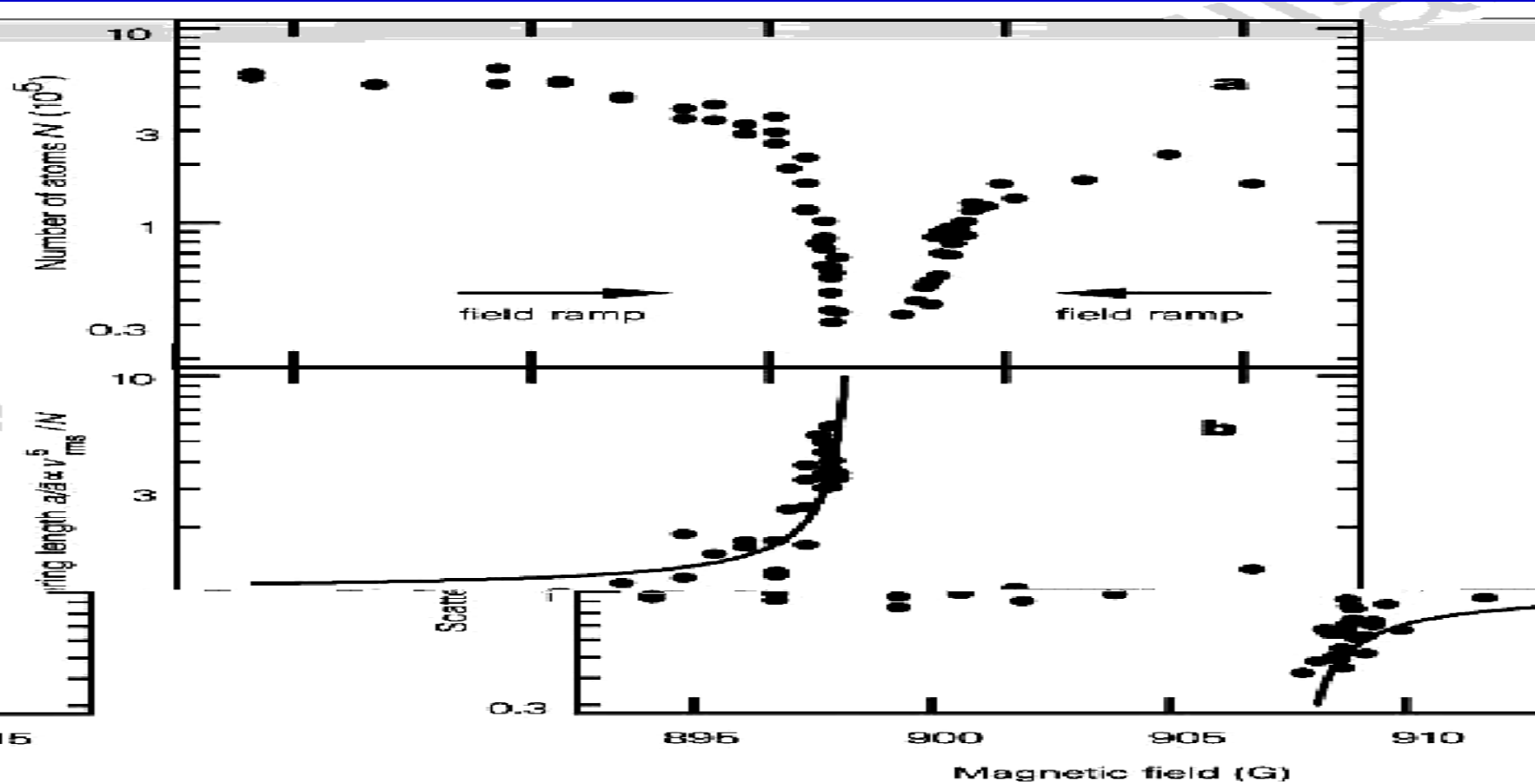


Fig. 1. Illustration of a Feshbach-resonant atomic collision. Two atoms, with a hyperfine state indicated by the arrow, collide and form a long-lived molecule with a different spin arrangement, which ultimately decays again into two atoms.

# 4.1. Strong interacting system

S. Inouye et al., Nature 392, 151 (1998).



using time-of-flight versus magnetic field. quickly crossing the m above. b, The released energy. The values of the are an uncertainty of

**Figure 2** Observation of the Feshbach resonance at 907 G absorption imaging. **a**, Number of atoms in the condensate versus magnetic field. Field values above the resonance were reached by quickly crossing the resonance from below and then slowly approaching from above. The released energy, together with the predicted shape (equation (1), solid line), is shown. The values of the magnetic field in the upper scan relative to the lower one have an uncertainty of  $<0.5$  G.

**Z. X. Liang, Z. D. Zhang, W. M. Liu,**

**Dynamics of a bright soliton  
in Bose-Einstein condensates**

**with time-dependent atomic scattering length  
in an expulsive parabolic potential,**

**Phys. Rev. Lett. 74, 050402 (2005).**

$$i\frac{\partial\psi(x,t)}{\partial t} + \frac{\partial^2\psi(x,t)}{\partial x^2} + 2\alpha(t)|\psi(x,t)|^2\psi(x,t) + \frac{1}{4}\lambda^2x^2\psi(x,t) = 0. \quad (1)$$

$$\begin{aligned} \psi &= \left[ A_c + A_s \frac{(\gamma \cosh \theta + \cos \varphi) + i(\alpha \sinh \theta + \beta \sin \varphi)}{\cosh \theta + \gamma \cos \varphi} \right] \\ &\quad \times \exp \left( \frac{\lambda t}{2} + i\varphi_c \right), \end{aligned} \quad (4)$$

where

$$\begin{aligned} \theta &= -\frac{[(k_0 + k_s)\Delta_R - \sqrt{g_0}A_s\Delta_I]}{2\lambda} [\exp(2\lambda t) - 1] \\ &\quad + \Delta_R x \exp(\lambda t), \\ \varphi &= -\frac{[(k_0 + k_s)\Delta_I + \sqrt{g_0}A_s\Delta_R]}{2\lambda} [\exp(2\lambda t) - 1] \\ &\quad + \Delta_I x \exp(\lambda t), \end{aligned} \quad (5)$$

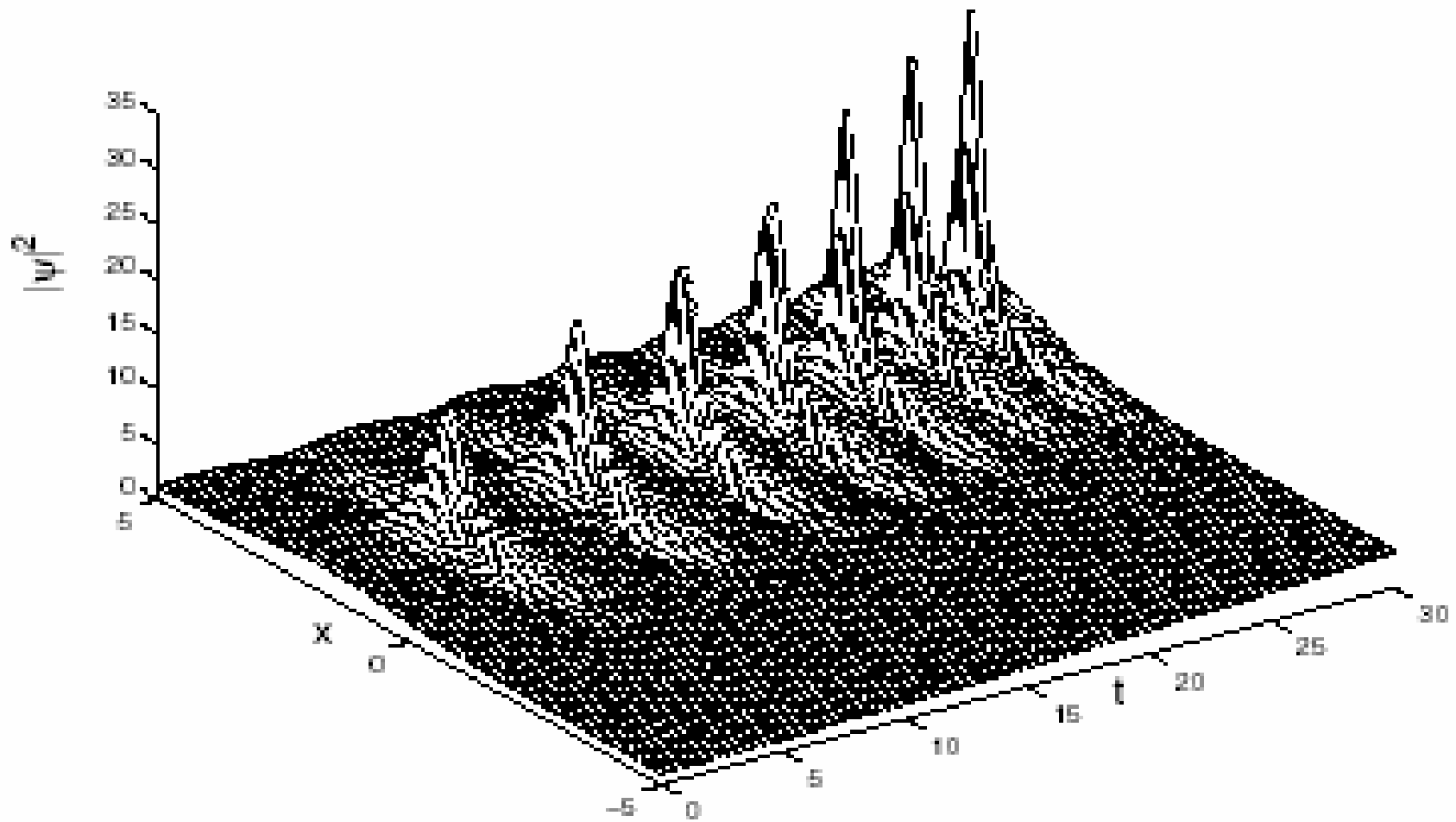


Figure 1: The dynamics of Feshbach resonance managed soliton in the expulsive parabolic potential given by Eq. (8). The parameters are given as follows:  $\lambda = 2 \times 10^{-2}$ ,  $g_0 = 0.25$ ,  $A_c = 1$ ,  $A_s = 2.4$ ,  $k_0 = 0.03$ ,

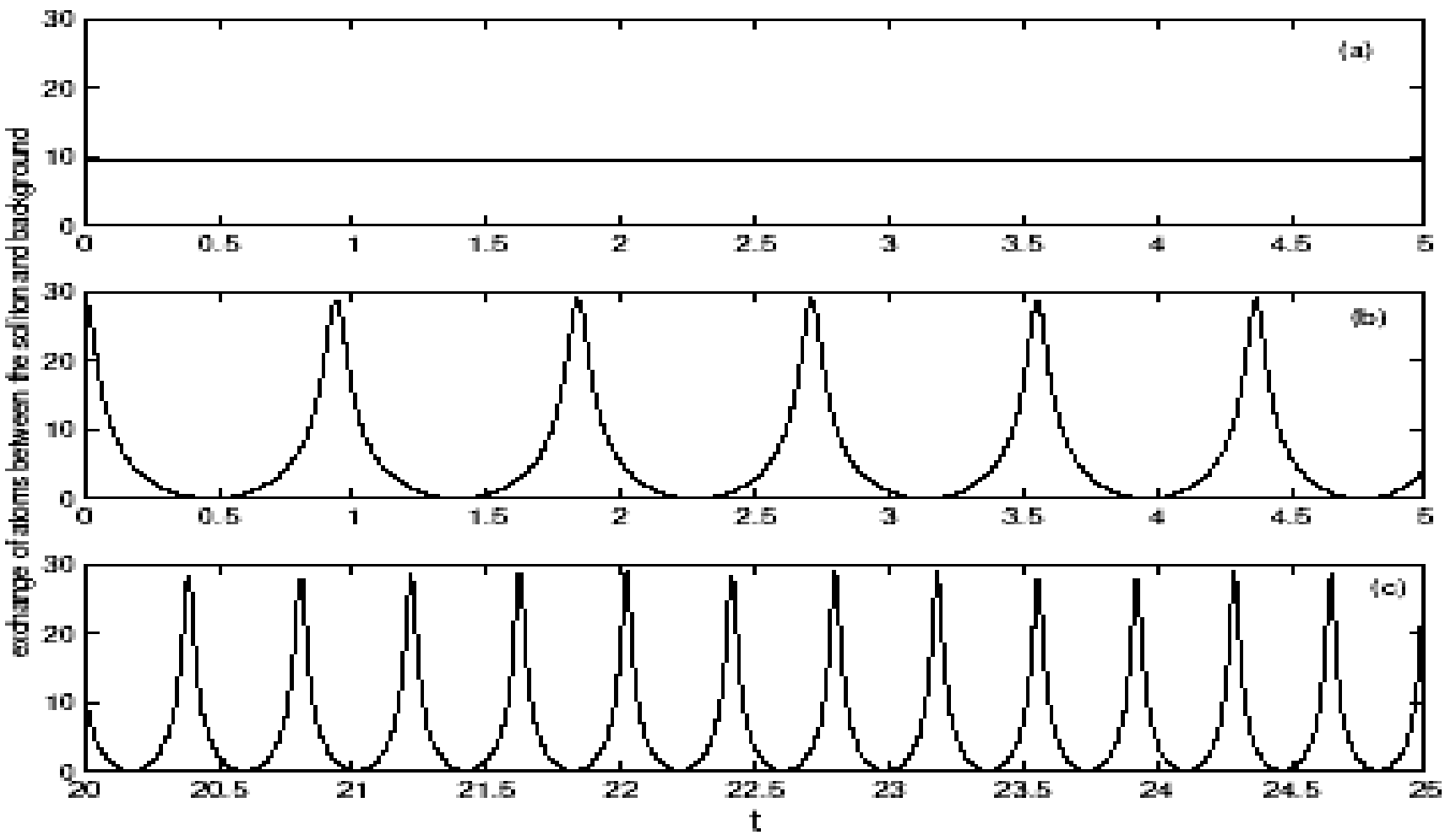


Figure 2: Time-periodic atomic exchange between the bright soliton and the background given by Eq. (13). The range of time is: (a) and (b)  $t=[0, 5]$ , (c)  $t=[20, 25]$ . The parameters are given as follows:  $\lambda = 0.02$ ,  $g_0 = 1$ ,  $A_s = 4.8$ , (a)  $A_c = 0$ , (b) and (c)  $A_c = 2.3$ .

## 4.2. Strong correlated bosonic system

$$\hat{H} = -J \sum_{\langle i,j \rangle} \hat{a}_i^\dagger \hat{a}_j + \sum_i \varepsilon_i \hat{n}_i + \frac{1}{2} U \sum_i \hat{n}_i (\hat{n}_i - 1), \quad (3)$$

## 4.3. Quantum Hall Effect

1985, Quantum Hall Effect, Nobel Prize  
in Physics

1998, Fraction Quantum Hall Effect,  
Nobel Prize in Physics

2003, Spin Hall Effect

# 5. Spinor BEC

J. Stenger, Nature 396, 345 (1998).

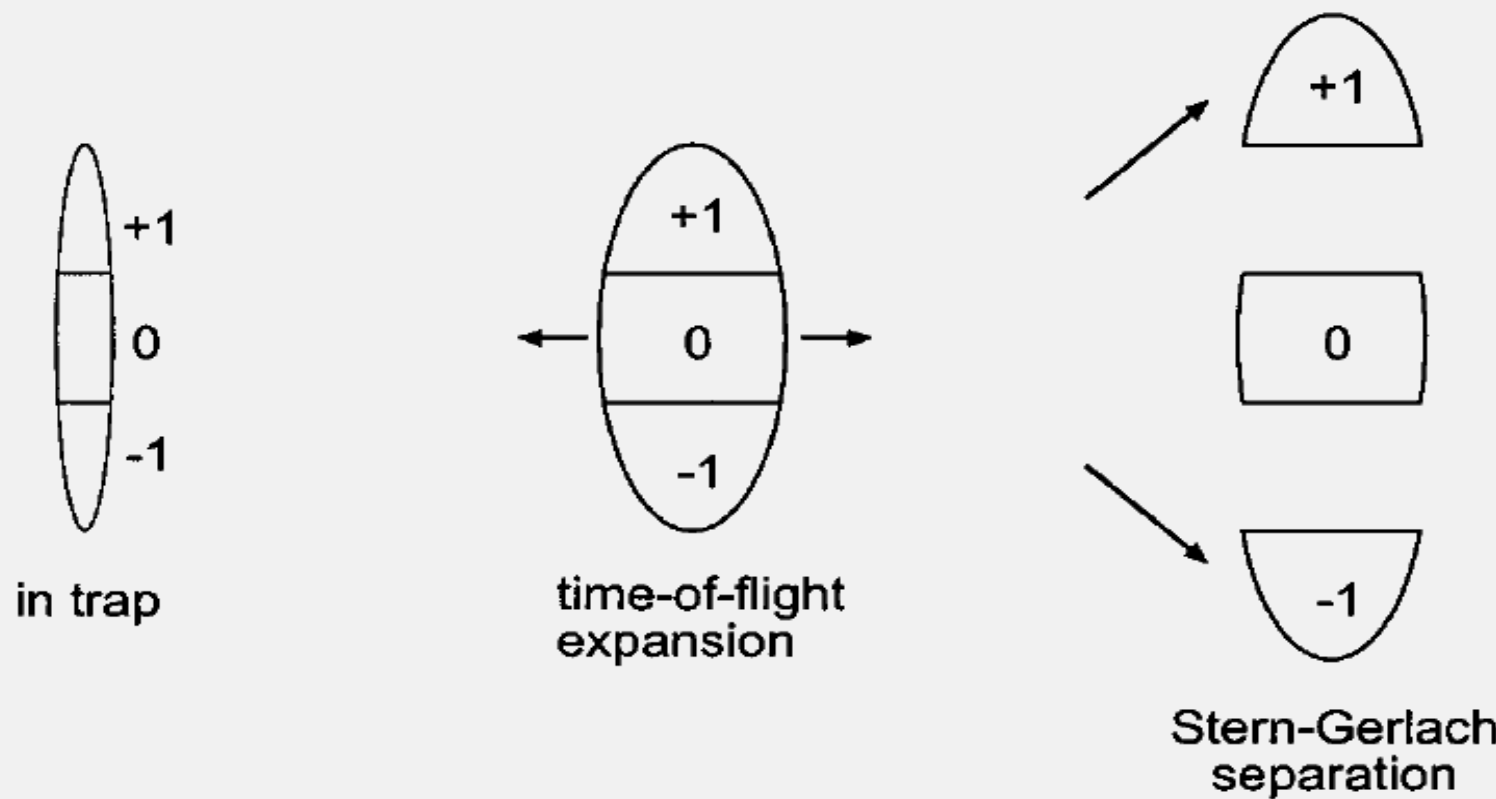
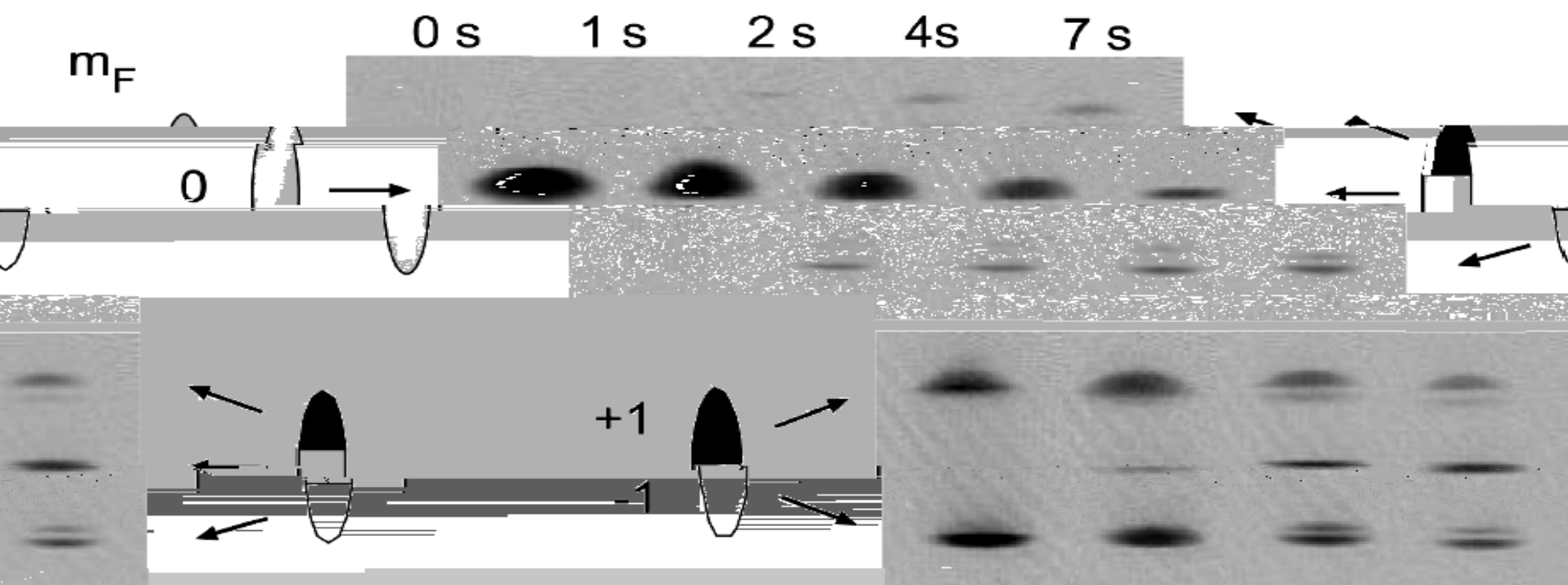


Fig. 21. Probing spinor condensates. After release from the elongated optical trap, the trapped spinor condensate expands primarily radially while maintaining the axial hyperfine distribution. A magnetic field gradient is then used to separate out the different components while preserving their shape. A subsequent absorption probe reveals the spatial and hyperfine distributions in the trap. From Ref. 53.

# Evolution time in the trap



Z.W. Xie, W.P. Zhang, S.T. Chui, W.M. Liu,

Magnetic solitons of  
spinor Bose-Einstein condensates  
in optical lattice,

Phys. Rev. A69, 053609 (2004).

Z.D. Li, P.B. He, L.Li, J.Q. Liang, W.M. Liu,

Soliton collision of  
spinor Bose-Einstein condensates  
in optical lattice,

Phys. Rev. A71, 053608 (2005).

**L. Li, Z.D. Li, B. A. Malomed, D. Mihalache, W. M. Liu,**

**Exact soliton solutions and  
nonlinear modulation instability  
in spinor Bose-Einstein condensates,**

**Phys. Rev. A 72, 033611 (2005).**

# **6. Boson-Fermion mixture**

**6.1. Collapse of attractive BEC**

**6.2. Collapse of Fermi gas**

**6.3. Boson-Fermion mixture**

# 6.1. Collapse of attractive BEC

C.E. Wieman, Nature 412, 295 (2001).

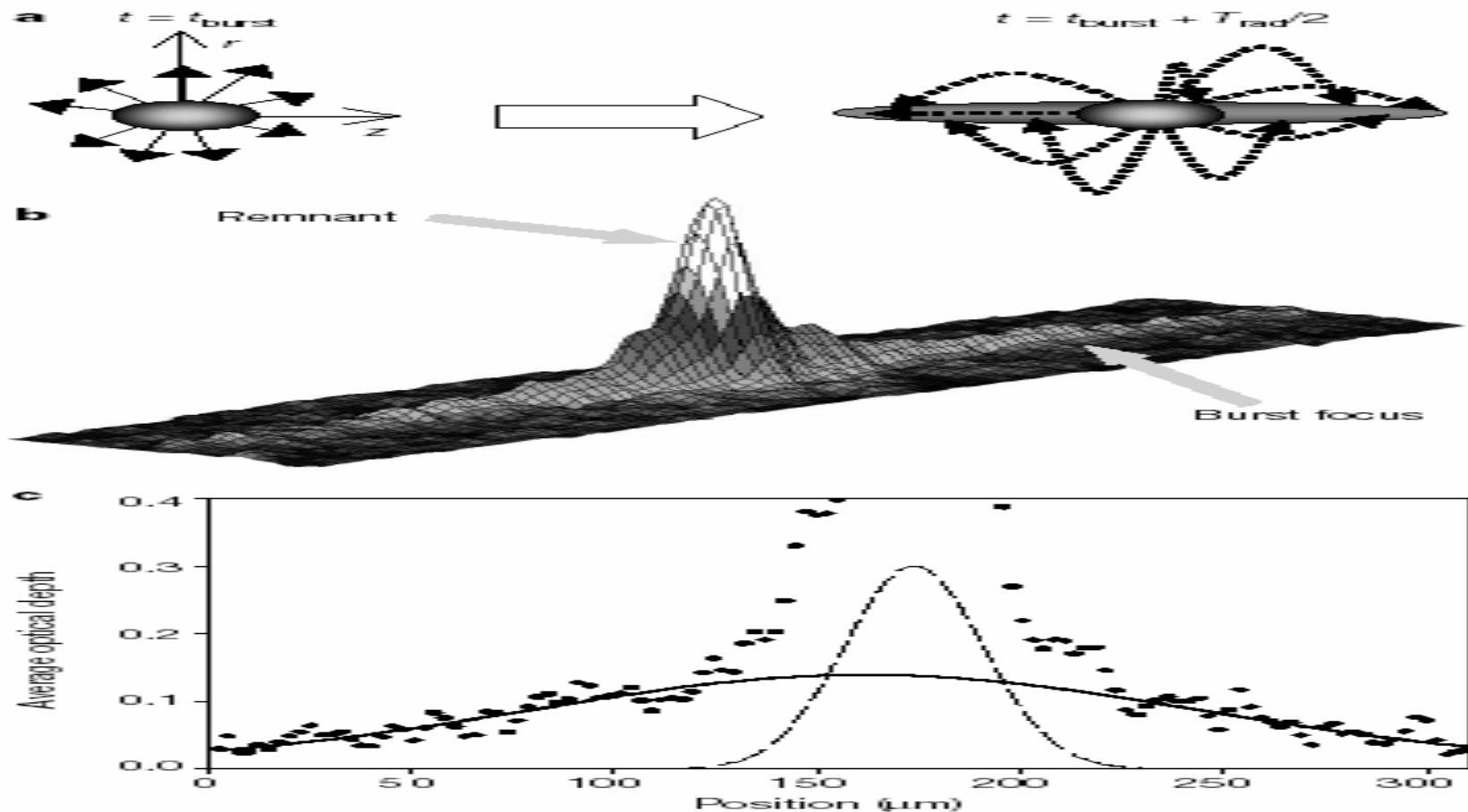
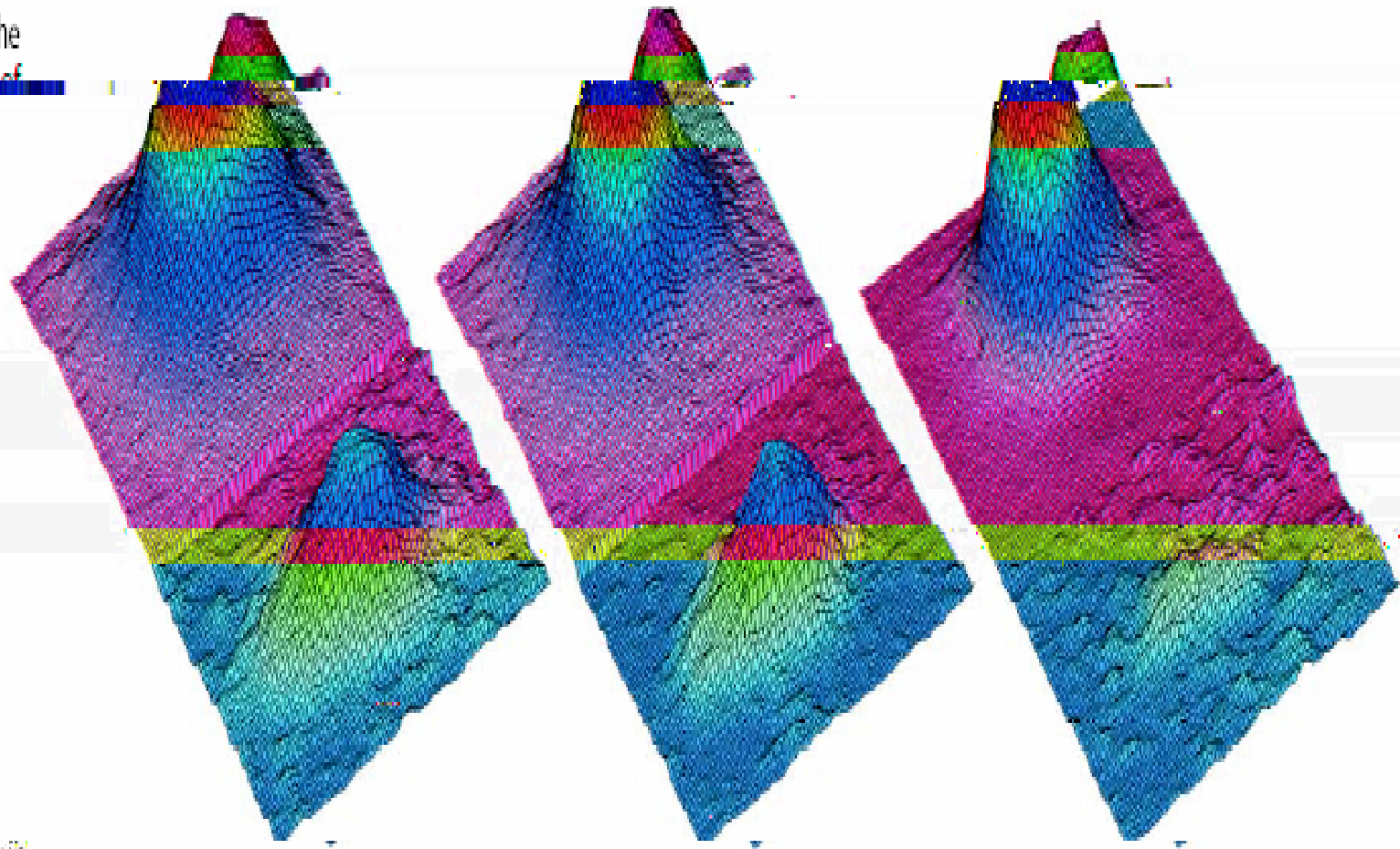


**Figure 3** A burst focus. **a**, Conceptual illustration of a radial burst focus.  $t_{\text{burst}}$  is the time at which the burst is generated and  $T_{\text{rad}}$  is the radial trap period. **b**, An image of a radial burst focus taken 33.5 ms after a jump from  $a_{\text{int}} = 0$  to  $-30a_0$  for  $N_0 = 10,000$ .  $T_{\text{rad}}/2 = 28.6$  ms, which indicates that the burst occurred 4.9(5) ms after the jump. The axial energy distribution for this burst corresponded to an effective temperature of 62 nK. The image is  $60 \times 310 \mu\text{m}$ . **c**, Radially averaged cross-section of **b** with a gaussian fit to the burst energy distribution. The central  $100 \mu\text{m}$  were excluded from the fit to avoid distortion in the fit due to the condensate remnant ( $\sigma = 9 \mu\text{m}$ ) and the thermal cloud ( $\sigma = 17 \mu\text{m}$ ). The latter is present in the pre-collapse sample due to the finite temperature, and appears to be unaffected by the collapse. The dashed line indicates the fit to this initial thermal component. We note the offset between the centres of the burst and the remnant. This offset varies from shot to shot by an amount comparable to the offset shown.

## 6.2. Collapse of Fermi gas

M. Inguscio, Science 297, 2240 (2001).

Fig. 2. False-color reconstruction of the density distribution of the Fermi (front) and Bose (back) gases during the evaporation procedure, as detected after a ballistic expansion of 4 ms for K and 9 ms for Rb. (Left) the BEC starts to form (middle) the BEC cloud and is coexisting with a relatively large Fermi gas; (right) as the BEC grows larger, the Fermi gas is only moderately depleted by inelastic collisions;



(right) when a quasi-pure condensate of  $10^5$  atoms has formed, the Fermi gas has already collapsed. The fermionic distributions have been vertically expanded by a factor of 3.

## 6.3. Boson - Fermion mixture

R.G. Hulet, Science 291, 2570 (2001).

$^7\text{Li}$

$^6\text{Li}$



## **7. BEC – BCS crossover**

**BEC:  $a > 0$ , bound molecular state**

**BCS:  $a < 0$ , fermionic atom pairs -**

**strong interaction**

BCS

BEC

weak coupling

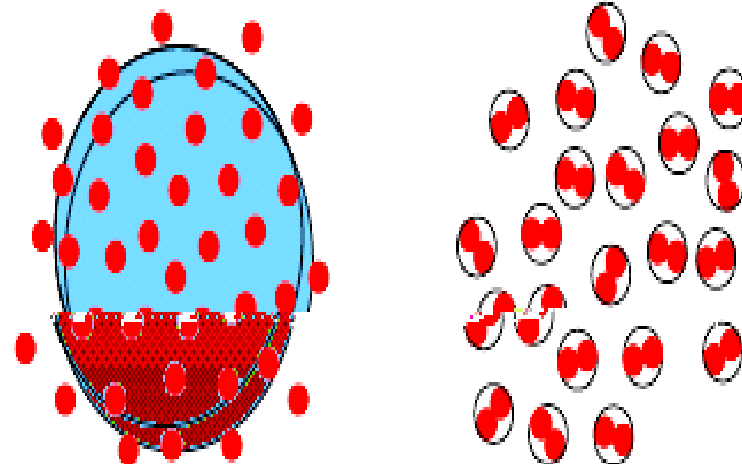
strong coupling

large pair size  
k-space pairing

small pair size  
r-space pairing

strongly overlapping  
Cooper pairs

ideal gas of  
preformed pairs



$$T^* = T_c$$

$$T^* \gg T_c$$

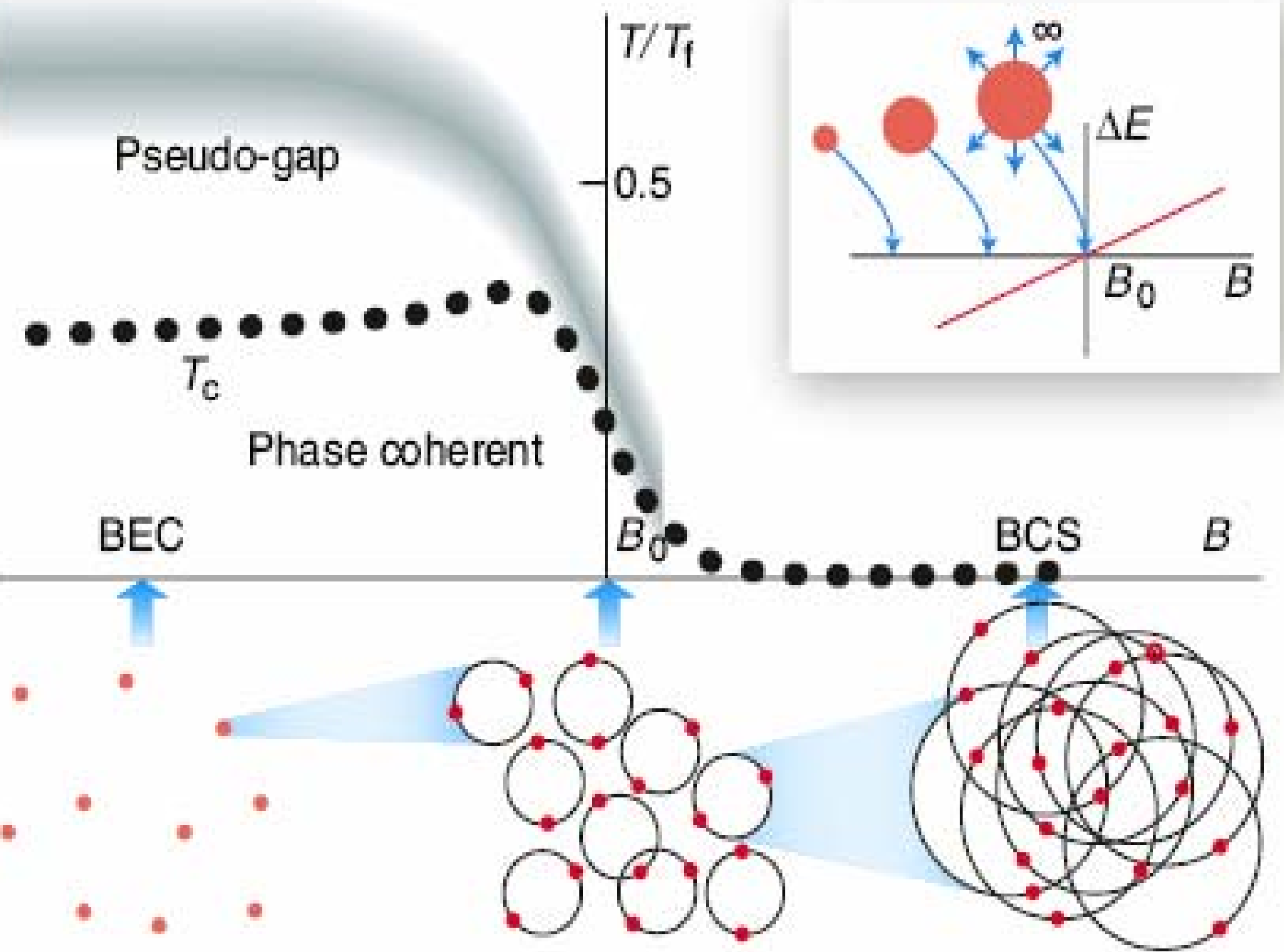
Fig. 1. Contrast between BCS and BEC based superfluids. Here  $T^*$  represents the temperature at which pairs form, while  $T_c$  is that at which they condense.

# BCS

Binding energy of pairs	$\approx$	Transition temperature	$\approx$	Fermi temperature
$10^{-5} \dots 10^{-4}$		normal superconductors		
$10^{-3}$		superfluid $^3\text{He}$		
$10^{-2}$		high $T_c$ superconductors		

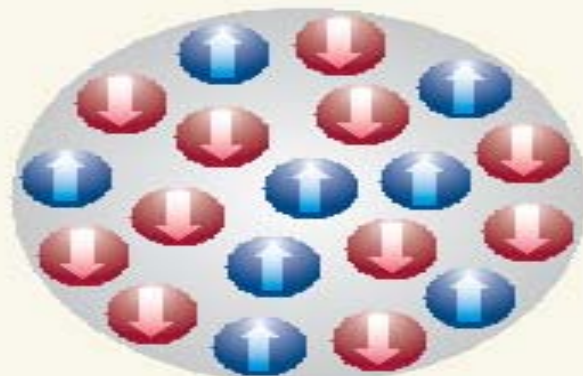
# BEC

Binding energy of bosons	$\approx$	$k_B$ BEC transition temperature
$10^5$		superfluid $^4\text{He}$
$10^{10}$		alkali BEC

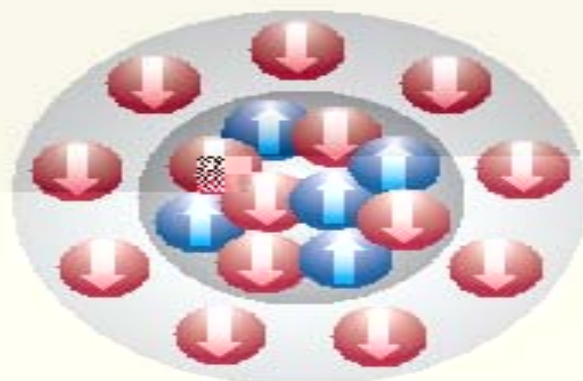


# 8. Spin polarized fermi gas

a



b



Sarma

(interior gap pairing)

Fulde-Ferrell-  
Larkin-Ovchinnikov  
(FFLO)

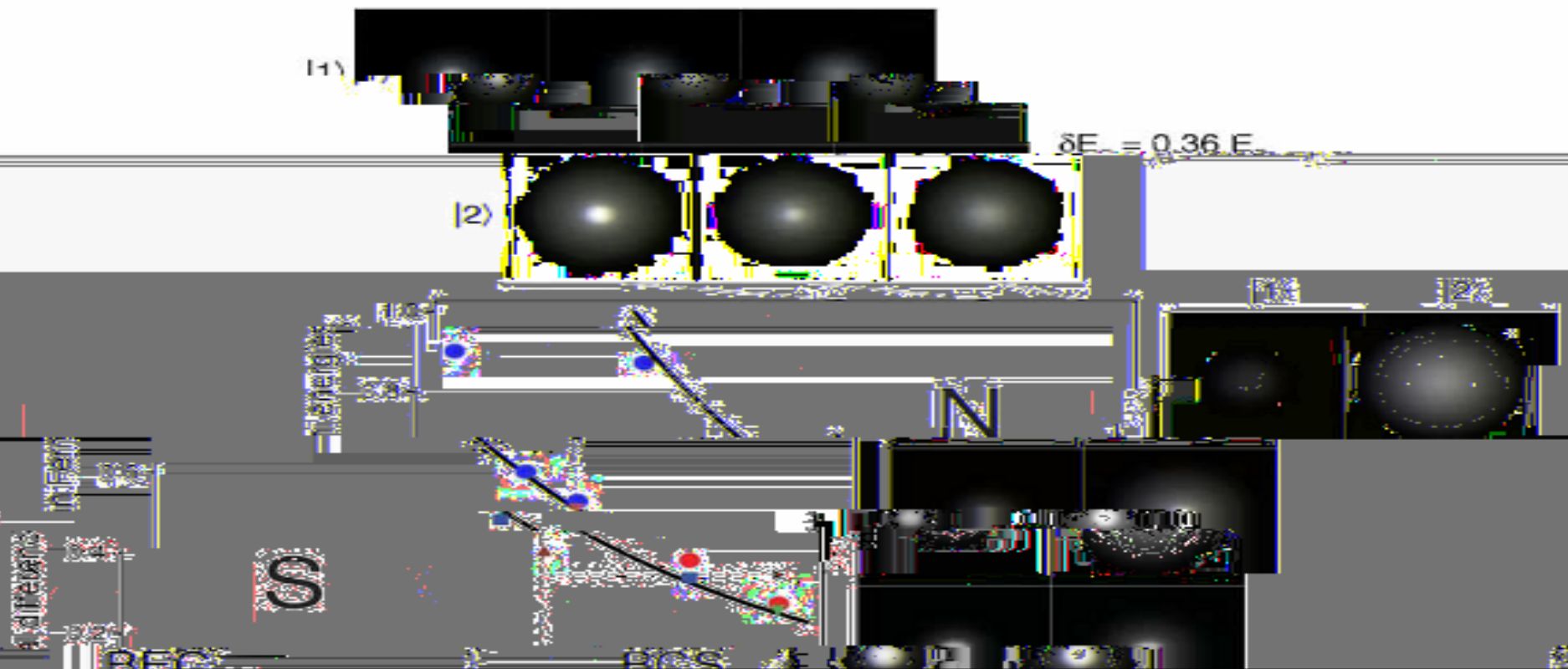
BCS

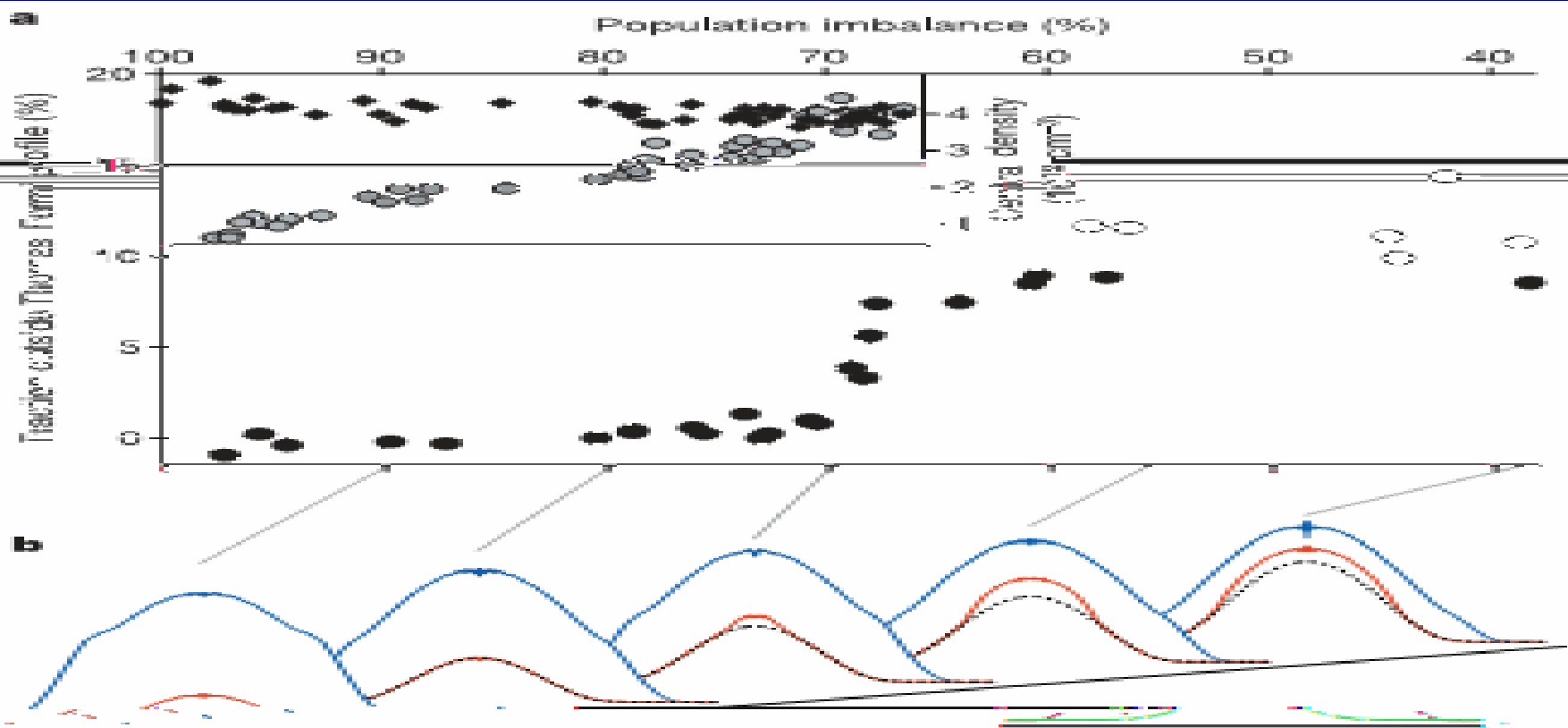
(SF)

(SFp)

(N)

Figure 1 | Changing shape. a, A homogeneous state of an unequal number of spin-up and spin-down atoms, such as that prepared by Zwierlein *et al.*





**Transition to superfluidity for decreasing**  
minority fraction. In the main panel, the ‘condensate fraction’ of excess minority atoms, not contained in the Fermi fit, versus population imbalance. The profiles of majority (blue) and minority (red) clouds, azimuthally averaged, for varying population imbalance in the minority component as the normal background (finite-temperature Thomas-Fermi fit, dotted lines). Below the critical imbalance  $\delta_c = 70\%$ , the condensate starts to form. The central density of the majority component decreases as the population imbalance increases, indicating that here the central densities were calculated from the size of the clouds, assuming local ballistic (hydrodynamic) motion of the minority clouds. The data points are averages of several independent

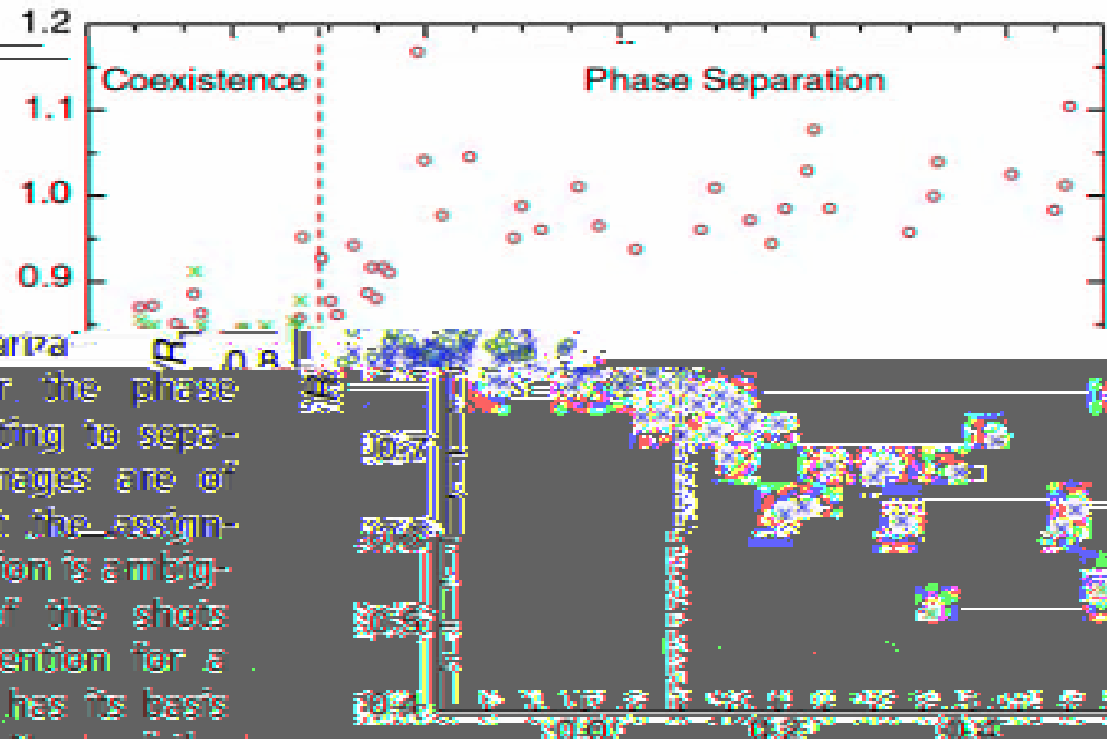
**Figure 3 | Quantum phase transition to superfluidity for decreasing population imbalance.** **a,** Main panel, the ‘condensate fraction’ of excess minority atoms, not contained in the Fermi fit, versus population imbalance on resonance. **b,** Column density of minority (red) clouds, azimuthally averaged, versus population imbalance. The condensate is clearly visible as the dense central feature on top of the normal-temperature Thomas-Fermi fit, dotted lines. At  $\delta_c = 70\%$ , the condensate starts to form. The central density of the majority component decreases as the population imbalance increases, indicating that here the central densities were calculated from the size of the clouds, assuming local ballistic (hydrodynamic) motion of the minority clouds. The data points are averages of several independent measurements.

**Fig. 3.**  $R/R_{TF}$  versus  $P$ . The ratios of the measured axial radius to that of a noninteracting T-F distribution are shown as blue open circles for state  $|1\rangle$  and as red crosses for state  $|2\rangle$ . The data combine 92 independent shots. The dashed line corresponds

to the estimated critical polarization,  $P_c = 0.09$ .

son,  $P_c = 0.09$ , for the phase transition from coexisting to separated phases. The images are of sufficient quality that the assignment of phase separation is ambiguous in only two of the shots represented. Our contention for a phase transition at  $P_c$  has its basis in statistical evidence: None of the 31 shots deliberately prepared as  $P = 0$  and only one with a measured  $P < 0.03$  is phase separated, whereas all but 11 are. The ratio of  $R/R_{TF}$  to the  $P_c$  vector is constant over our statistical range of measurement of  $P$ . Although fluctuations in absolute probe detuning lead to 15% uncertainty in  $P$ , we estimate the uncertainty in a single measurement of  $P$  to be standard deviation of measurements of  $P$  for distributions prepared as  $P = 0$ . For distributions, we find no significant systematic shift in detection of relative number. The ratio  $R/R_{TF}$  is estimated to be 2.5%, due mainly to the uncertainty in measurement in  $R/R_{TF}$  for state  $|2\rangle$  grows with increasing  $P$  because of greater uncertainty of  $R$  with decreasing  $P$ .

two shots with  $P > P_c$  and the 10 with  $P < P_c$ . The uncertainty in total resulting in lower 5%, which is the 1%. Also from these the uncertainty in preparing  $P_c$  (20). The uncertainty in the fitted



© 2006 American Physical Society

# 9. Magnon BEC

Science 298, 760 (2002).

## 9.1. Magnon BEC

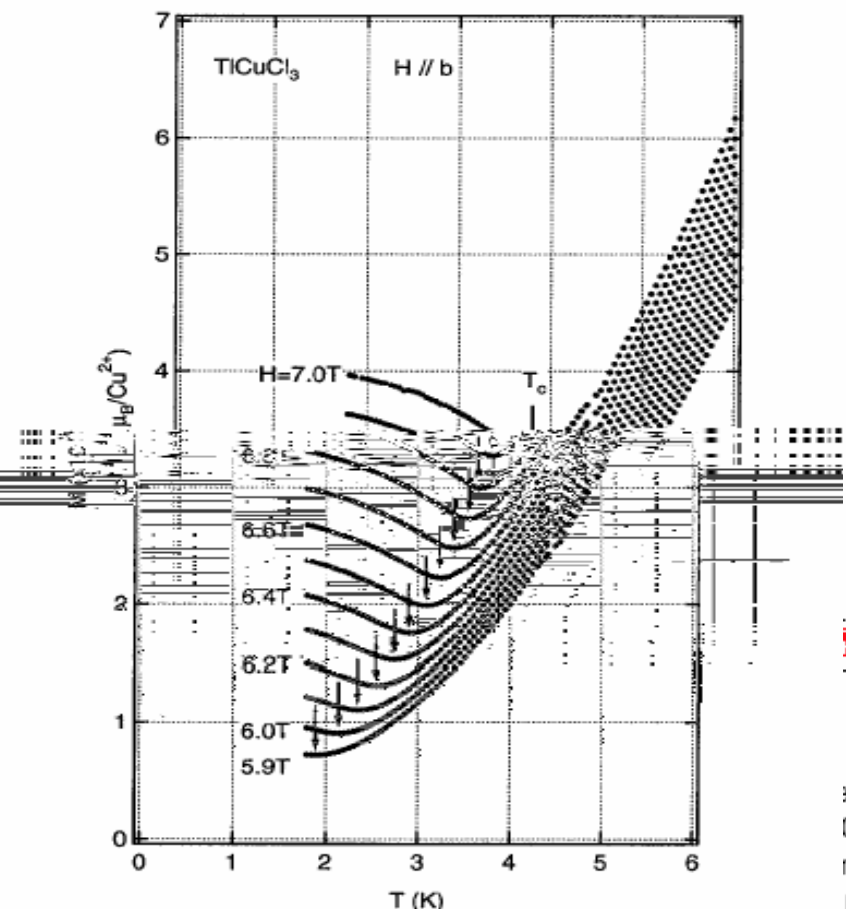


FIG. 2. The low-temperature magnetizations of  $\text{TiCuCl}_3$  measured at various external fields for  $H \parallel b$ .

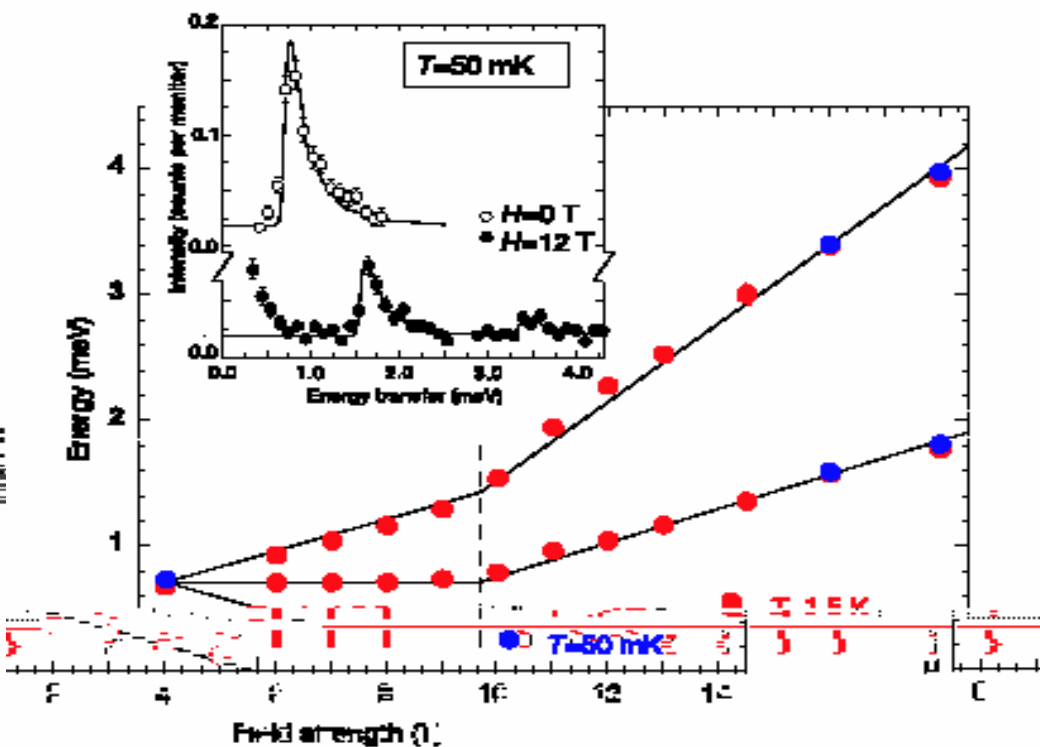
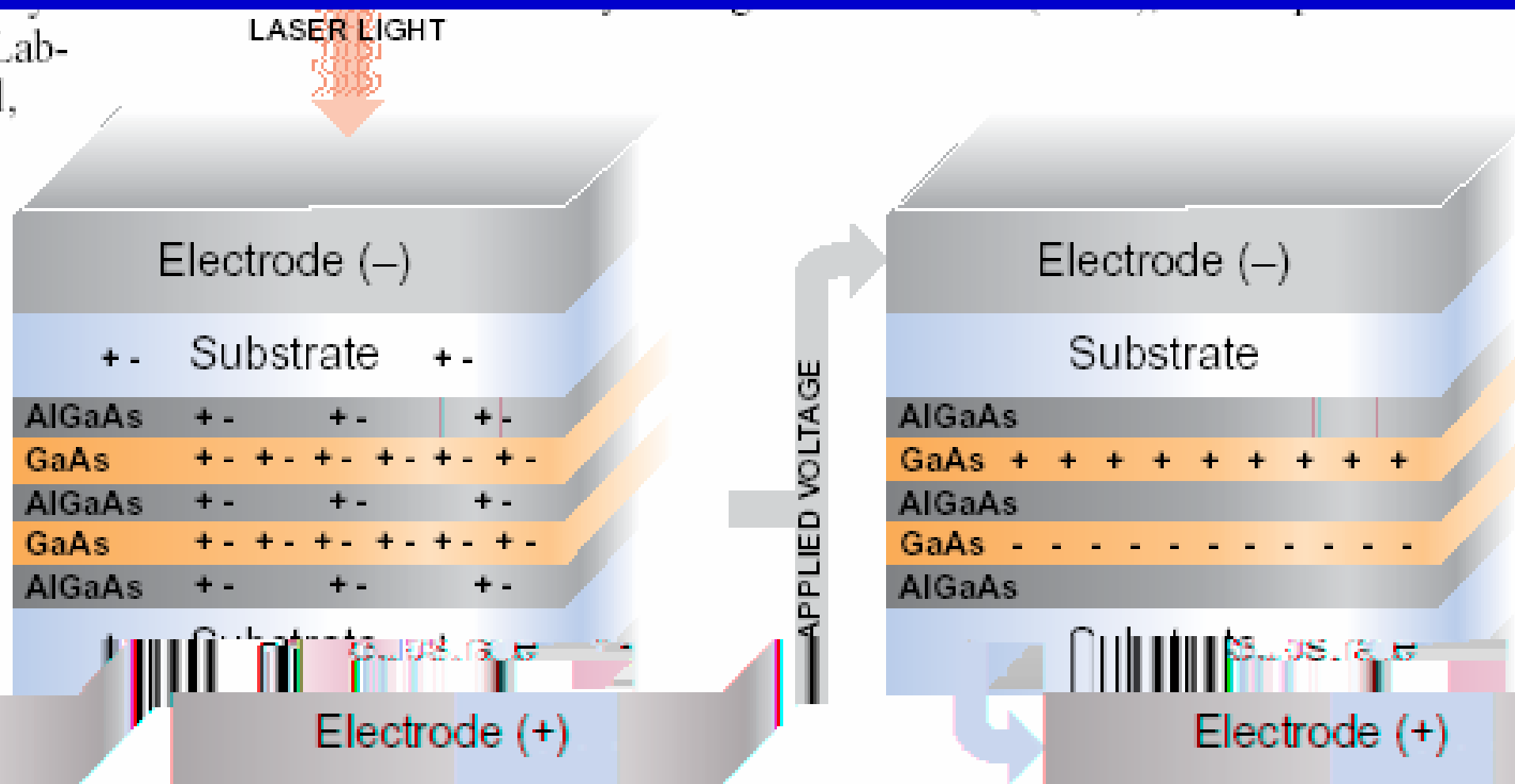


Figure 2 Dependence of magnetic excitation energy measured in  $\text{TiCuCl}_3$  at  $T = 1.5 \text{ K}$  (red symbols) and  $T = 50 \text{ mK}$  (blue symbols) and  $T = 50 \text{ mK}$  (blue symbols). Data are extracted from least-squares fits to the neutron scattering spectra (inset), curves reflect a Zeeman model. The field  $H = H_c$  is denoted by the dashed boundary. Comments and interpretations are given in the text.

Figure 2 Dependence of magnetic excitation energy measured in  $\text{TiCuCl}_3$  at  $T = 1.5 \text{ K}$  (red symbols) and  $T = 50 \text{ mK}$  (blue symbols). Data are extracted from least-squares fits to the neutron scattering spectra (inset), curves reflect a Zeeman model. The field  $H = H_c$  is denoted by the dashed boundary. Comments and interpretations are given in the text.

## 9.2. Exciton BEC

Science 300, 1871 (2003).

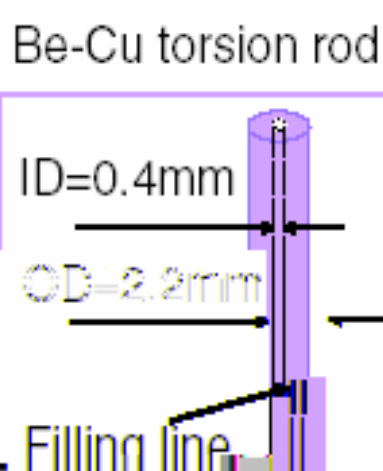


BEC in a semiconductor? Laser produces pairs of electrons (-) and holes (+) a BEC. Trapped in low-energy layers (right), charges form excitons that may condense into

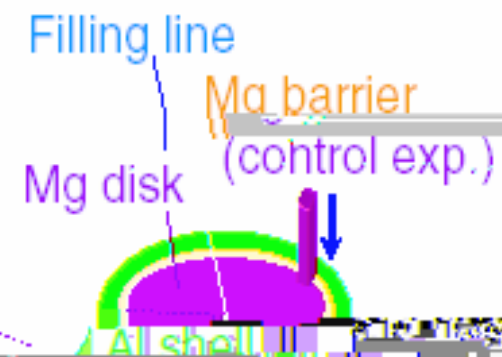
# 9.3. Superflow in Solid Helium

M. Chan, Science 305, 1941 (2004).

Fig. 1. Torsional oscillators: The cylindrical drive and detection electrodes are coupled capacitively to the two planar electrodes attached as fins on the two sides of the cylindrical torsion cell. Oscillation of the torsion cell induces a voltage on the detector electrode. This voltage enters a lock-in amplifier to keep the oscillation in resonance. The outside diameter, width, and height of the torsion cell in the barrier-free

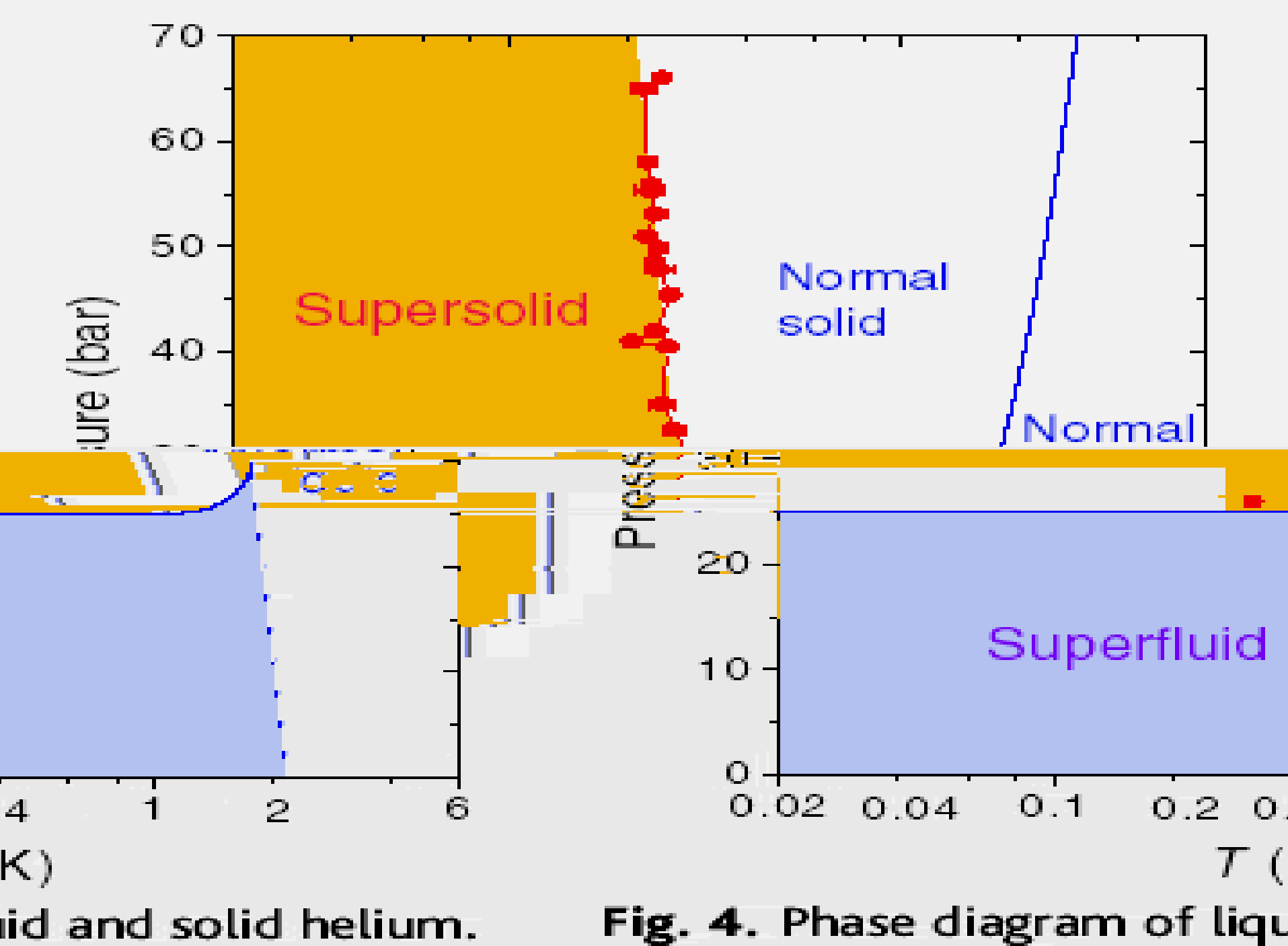


Torsion cell with helium in annulus



free torsion cell are 10 mm, 0.63 mm, and 5 mm, respectively. The mechanical quality factor of the oscillator is  $2 \times 10^6$ , allowing the determination of the resonant period to 0.2 ns out of a resonant period of 1 ms. The outside diameter, width, and height of the (blocked) channel of a second torsion

cell with the barrier are 15 mm, 1.1 mm, and 5 mm, respectively. The mechanical quality factor and period precision values are similar to those of the barrier-free



# **10. Application**

**10.1. Atomic laser**

**10.2. Atom clock**

**10.3. Interferometer (microgravity)**

**10.4. Waveguide**

**10.5. BEC on chip**

**10.6. Quantum tweezer**

**10.7. Information storage**

**10.8. Quantum computer**

**10.9. Four-wave mixing**

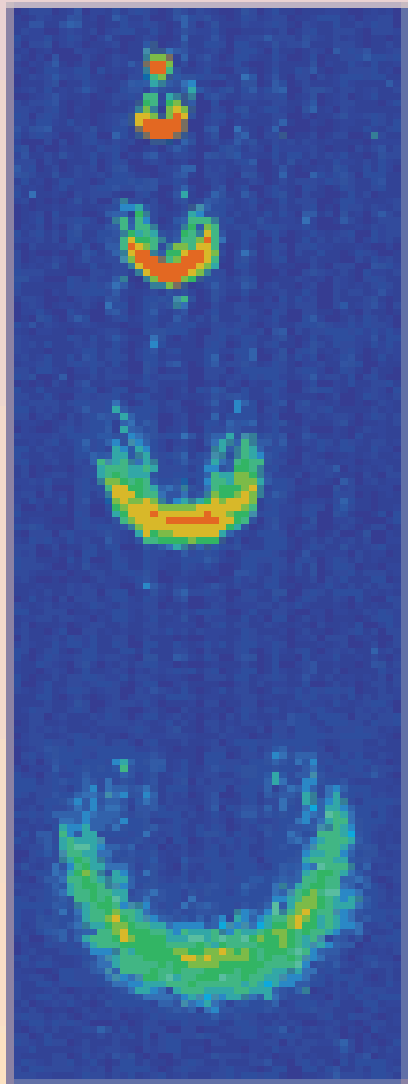
**10.10. Reducing light speed**

**10.11. Superradiance**

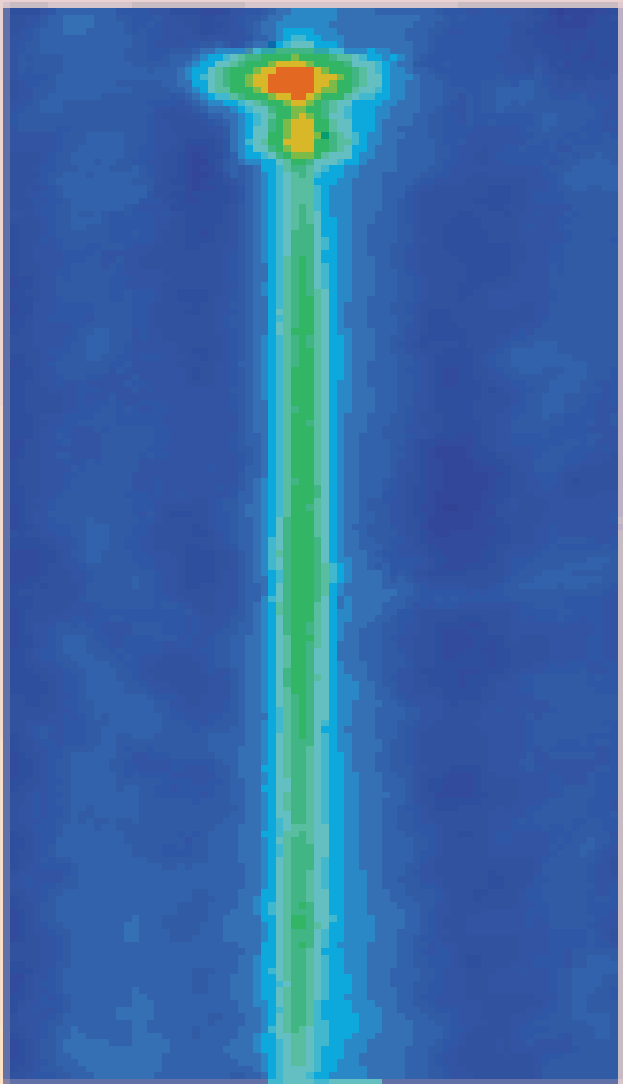
**10.12. Supernova**

# 10.1. Atom laser

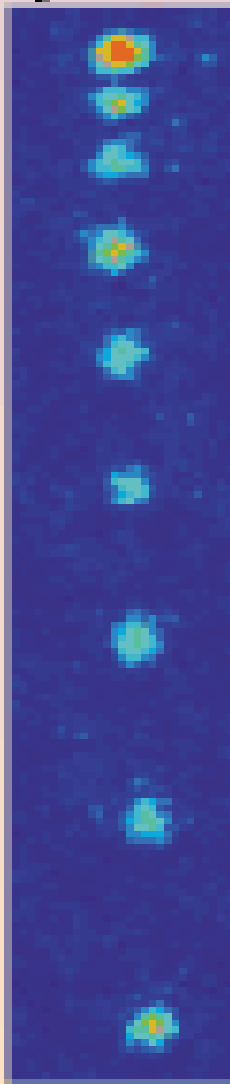
Atom Laser Gallery



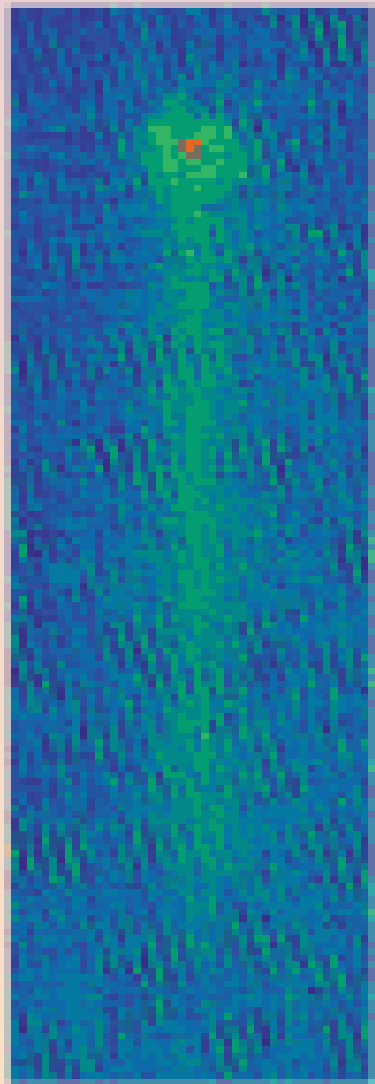
MIT



Munich



Yale



NIST

## 10.2. Atom clock

**Figure 3** Atom clocks. The first caesium atomic clock, built by Jerrold Zacharias in 1953. Zacharias' team at the Massachusetts Institute of Technology developed the first atomic beam maser, which was used to measure the frequency of the hyperfine transition in a beam of caesium atoms. This frequency was then used to stabilize a laser source, which in turn provided the light source for the clock. The clock had an accuracy of about 1 part in  $10^9$ .



## 10.3. Atom interferometer (microgravity)

M. A. Kasevich, Science 298, 1363 (2002)



## 10.3. Interferometer

J. Denschlag et al., Science 287, 97 (2000).

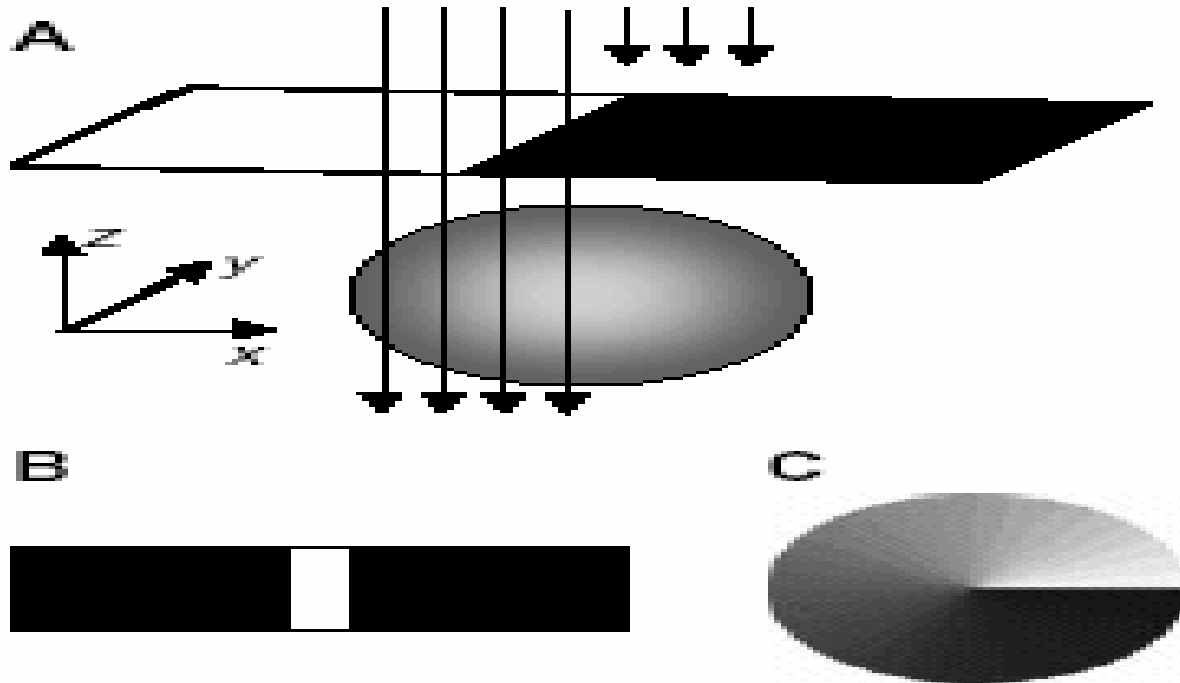


**Fig. 1. (A)** Writing a phase step onto the condensate. A far-detuned uniform light pulse projects a mask (a razor blade) onto the condensate. Because of the light shift, this imprints a phase distribution that is proportional to the light intensity distribution. A lens (not shown) is used to image the razor blade onto the condensate. The mask in (B) writes a phase stripe onto the condensate. The mask in (C) imprints an azimuthally varying phase pattern that can be used to create vortices.

# 10.4. Waveguides

Science 298, 1363 (2002)

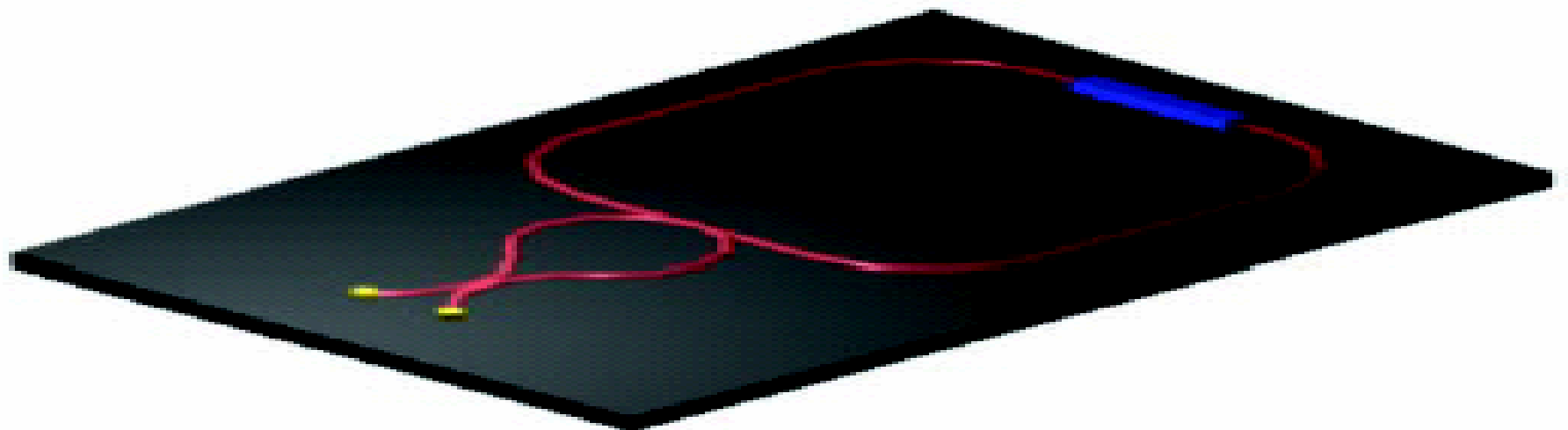


**Fig. 3.** Schematic of a possible geometry for a waveguide Sagnac-effect atom gyroscope. An atom gain element (blue) feeds a loop waveguide structure (red). Atoms are extracted and detected using correlated-state techniques to achieve sub-shot-noise limited detection (yellow). The past year has seen substantial progress in the development of each relevant element. A loop 10 cm by 10 cm might achieve a  $10^6$ -fold improvement in sensitivity to rotations for intermediate acquisition bandwidths (tens of seconds), and a  $10^4$ -fold improvement for high frequencies (less than 1 s). The long-term stability and accuracy are difficult to project.

# 10.5. BEC on chip

Nature 413, 498 (2001).

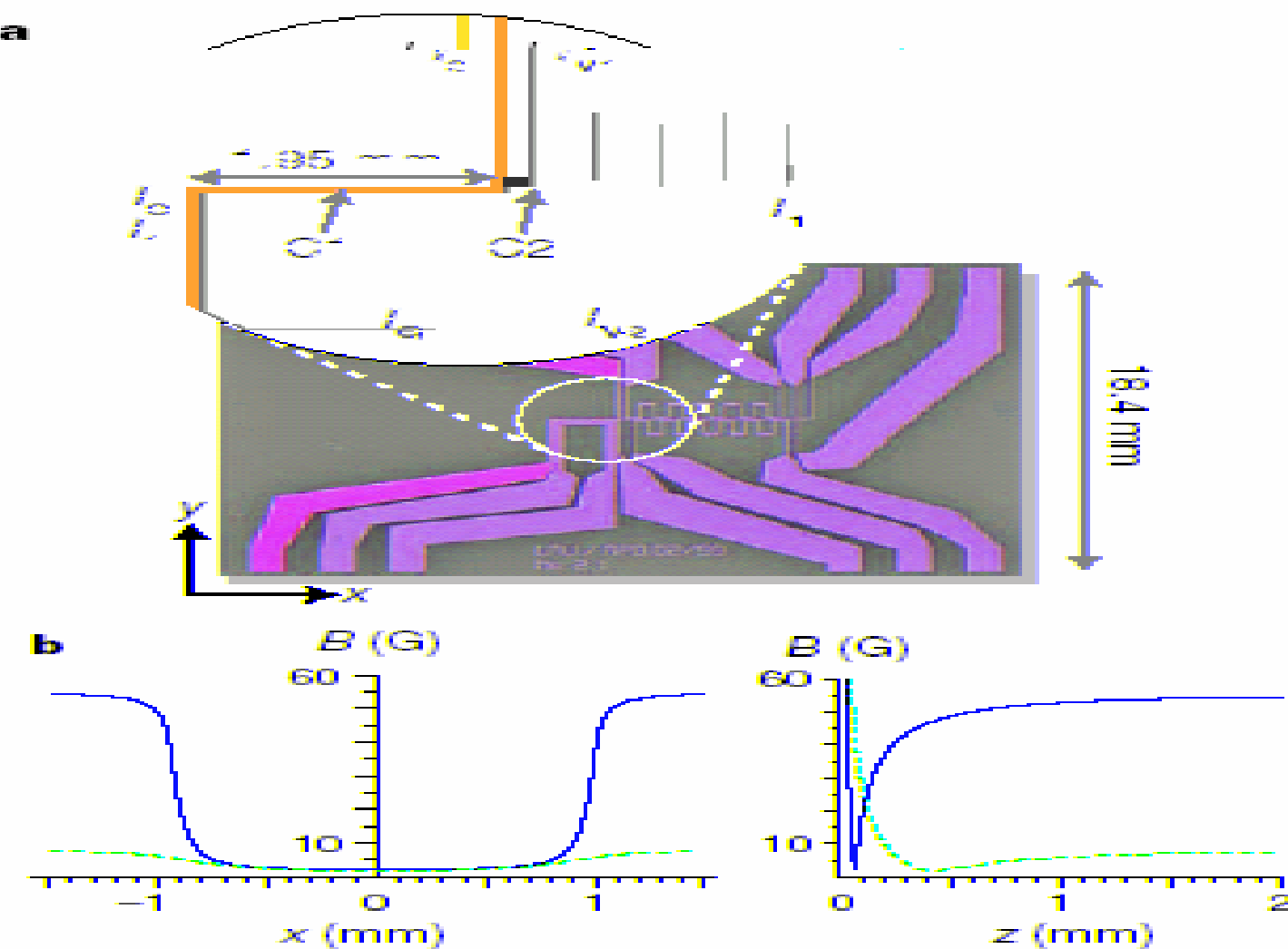
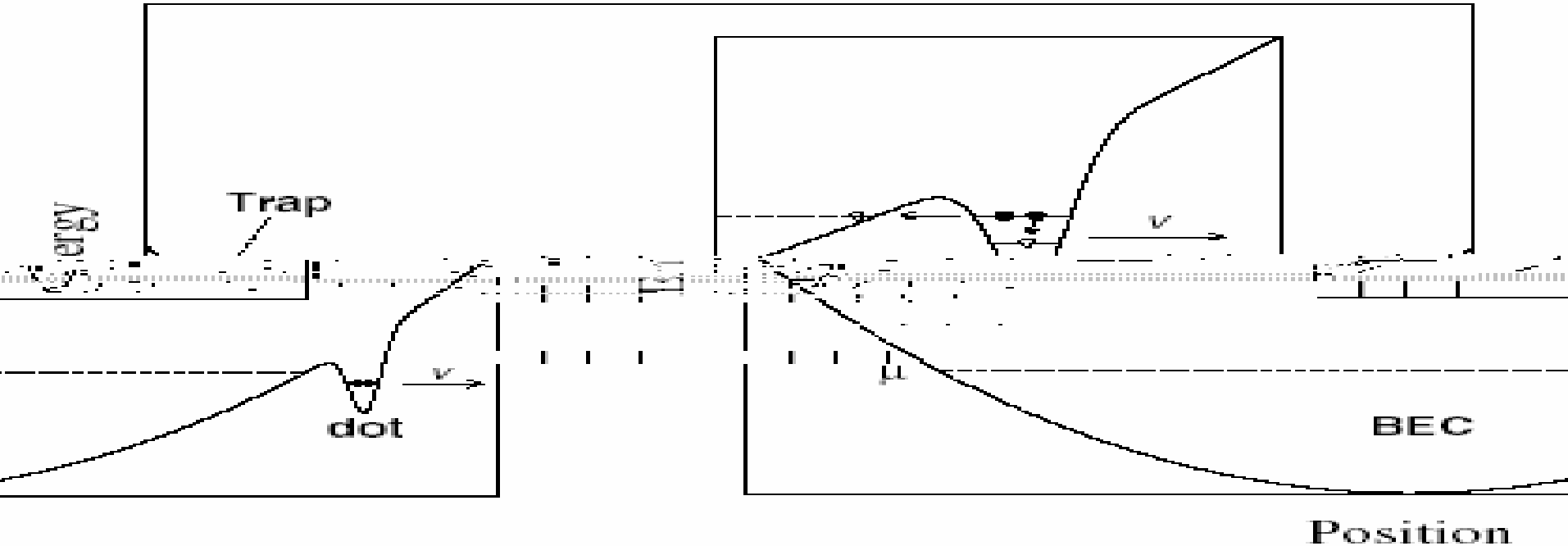


**Figure 1** The chip and the magnetic potentials that it creates. **a**, Layout of the lithographic gold wires on the substrate. The inset shows the relevant part of the conductor pattern. **b**,  $I_0$ ,  $I_{v1}$  and  $I_{v2}$  create the various magnetic potentials for trapping (see **b**) and transport, as described in the main text.  $I_0$  is used only during trap loading (intermediate MOT step<sup>5</sup>).  $I_{v1}$  and  $I_{v2}$  generate a double-well potential for trapping.  $I_{v1} = 2.4$  for two different values of the external magnetic field.

# 10.6. Quantum tweezers (loading single atom)

Nature 411, 1024 (2001); Science 293, 278 (2001); Phys. Rev. Lett. 89, 070401 (2002).

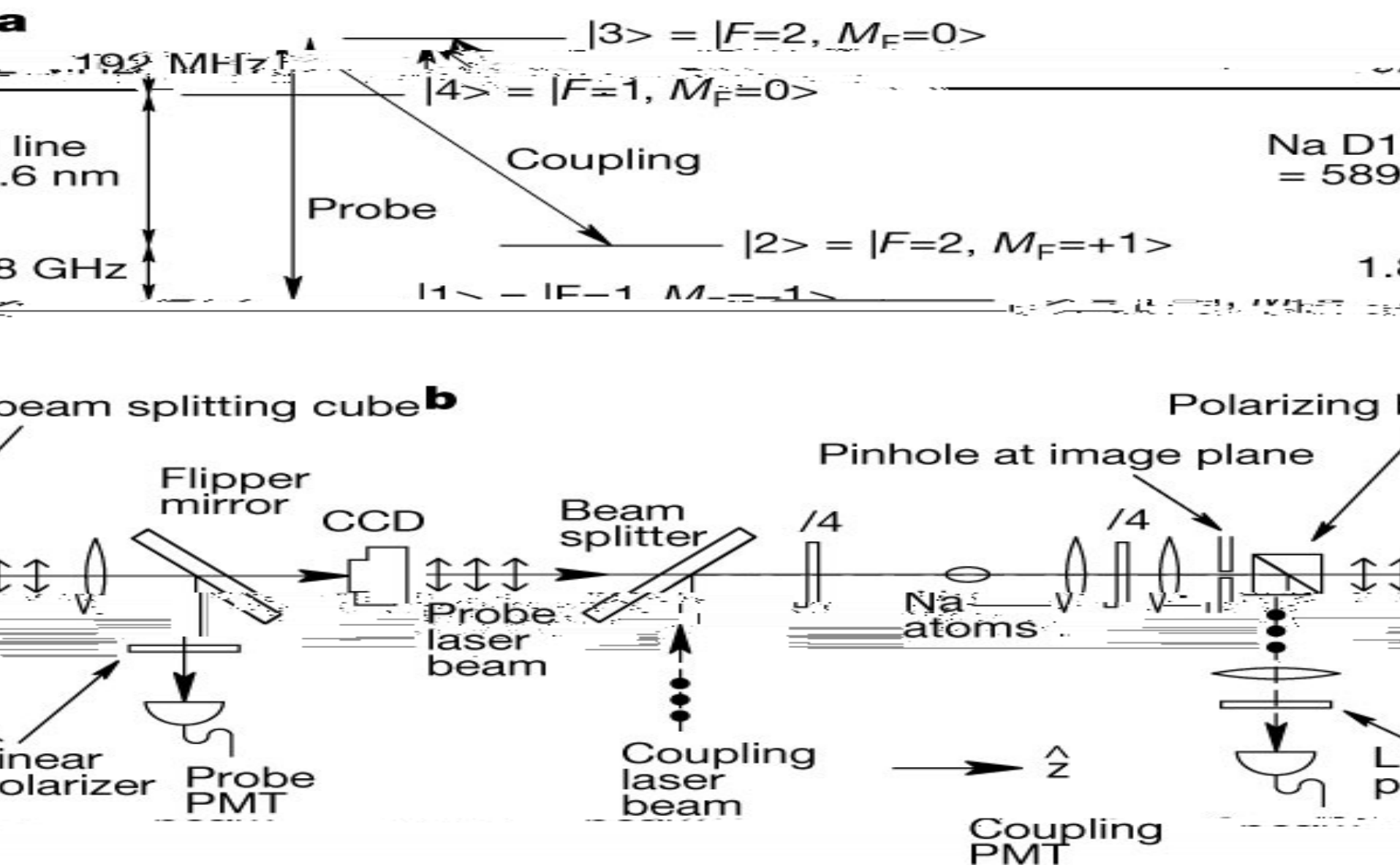


ves out of a trapped  
e inset illustrates that  
urther away from the  
e atoms matches the  
If one of the atoms is  
of the dot is lowered,  
e lost atom. Thus, no  
to the condensate at

FIG. 1. A quantum dot (tweezer) moves through a BEC (reservoir) with the speed of  $v$ . The trap potential is shown on the left. As the dot moves further away from the trap center such that the energy of the trap exceeds the chemical potential  $\mu$  of the condensate, an atom can tunnel into the BEC, the energy level of which due to the absence of repulsion from the other atom has a chance of leaking back to the trap at this position.

# 10.7. Information storage

C. Liu et al., Nature 409, 490 (2001).



# 10.8. Quantum computer and entanglement

Nature 409, 63 (2001).

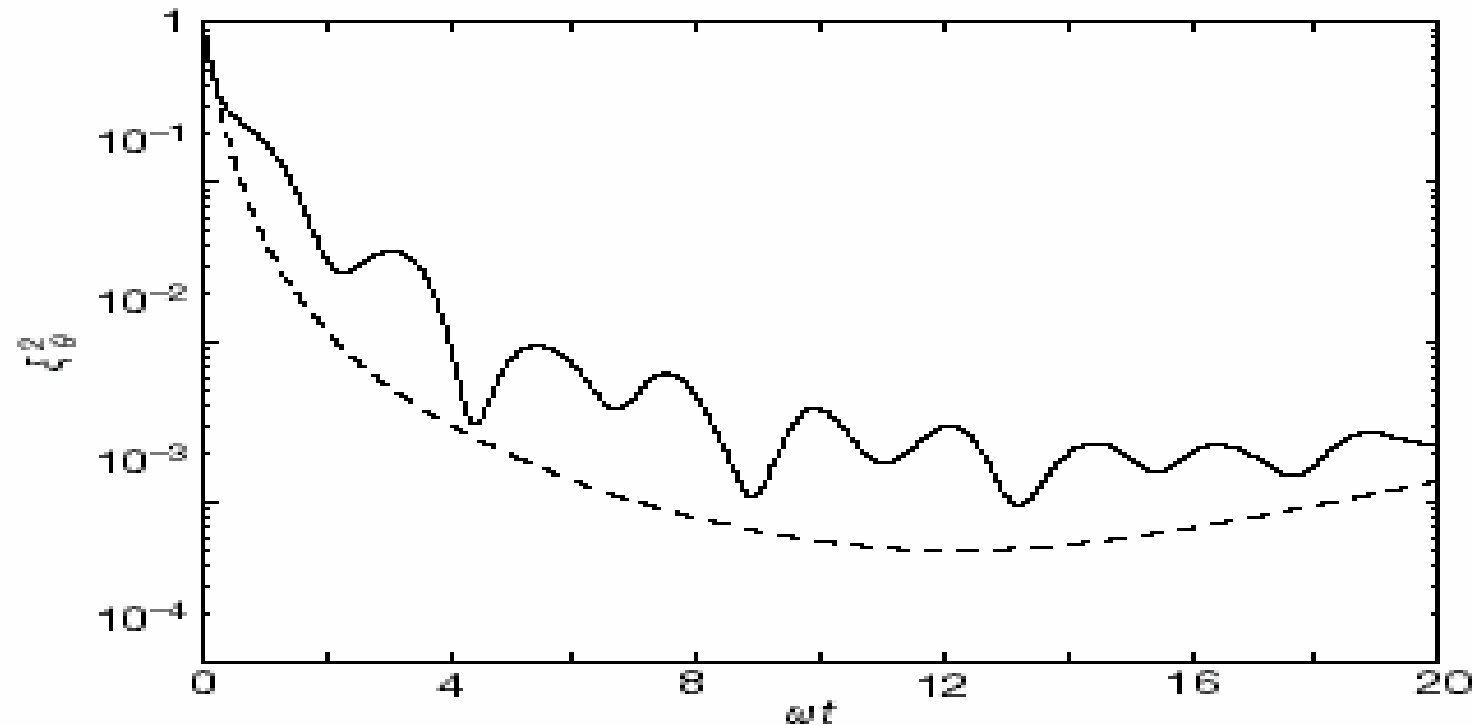
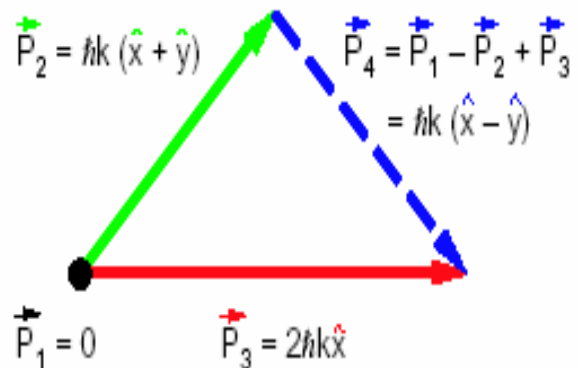


**Figure 1** Reduction in the squeezing parameter  $\xi^2$ . A fast  $\pi/2$  pulse between two internal states is applied to all atoms in the condensate. The subsequent free evolution with time results in a strong squeezing of the total spin. The angle  $\theta$  is chosen such that  $\xi_\theta^2$  is minimal. The solid line shows the results of a numerical integration (see text). For numerical convenience we have assumed a spherically symmetric potential  $V(r) = m\omega^2 r^2/2$ . The parameters are  $a_{ss}/d_0 = 6 \times 10^{-3}$ ,  $a_{bb} = 2a_{sb} = a_{ss}$ , and  $N = 10^6$ . The dashed curve shows the squeezing obtained from the hamiltonian  $H_{\text{spin}} = \hbar\chi J_z^2$ . The parameter  $\chi$  is chosen such that the reduction of  $\langle J_x \rangle$  obtained from the solution in ref. 7 is consistent with the results of ref. 11.

# 10.9. Four-wave mixing

L. Deng et al., Nature 398, 218 (1999).

a Lab frame:



b Moving frame:

$$\vec{v} = \frac{\hbar k}{M} \hat{x}$$

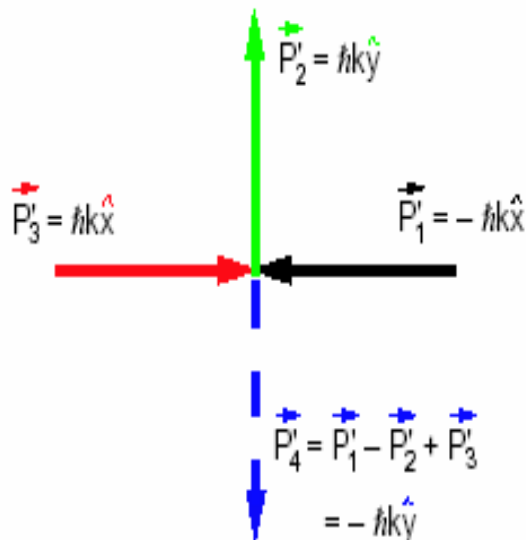


**Figure 1** Momentum-energy conservation for 4WM and the bosonic stimulation viewpoint in a moving frame. **a**, Momentum conservation,  $\vec{P}_4 = \vec{P}_1 - \vec{P}_2 + \vec{P}_3$  (equivalent to phase-matching in optical 4WM), in the laboratory frame. For clarity, over-arrows indicate vectors. Energy conservation requires  $\vec{P}_4^2 = \vec{P}_1^2 - \vec{P}_2^2 + \vec{P}_3^2$ . **b**, It is always possible to view matter 4WM in a frame moving with velocity  $\vec{v}$  such that the three input momenta have the same magnitude, and two are counter-propagating. Then, in our case two atoms in momentum states  $\vec{P}'_1 = -\hbar k \hat{x}$  and  $\vec{P}'_3 = -\hbar k \hat{x}$  are bosonically stimulated by wavepacket  $\vec{P}'_2 = -\hbar k \hat{y}$  to scatter into momentum states  $\vec{P}'_3$  and  $\vec{P}'_4 = -\vec{P}'_2 = -\hbar k \hat{y}$ . We note that the energy and momentum conditions are satisfied if the momentum of the reaction is  $\vec{P}'_2$ . The 4WM wavepacket is source-resonant (no loss of energy, no momentum and particle-number conservation) while atoms are stimulated into the final momentum state  $\vec{P}'_4$ . Thus 4WM can be viewed as the annihilation of momentum states  $\vec{P}'_1$  and  $\vec{P}'_3$  and the creation of momentum states  $\vec{P}'_3$  and  $\vec{P}'_4$  (the minus signs in the energy and momentum conditions are attached to the state that gains atoms). It is this bosonic stimulation of scattering that mimics the stimulated emission of photons from an optical nonlinear medium. Alternatively, by choosing a frame of reference in which  $\vec{P}'_1 = -\vec{P}'_2$  (or  $\vec{P}'_2 = -\vec{P}'_3$ ), 4WM can also be viewed as matter-wave Bragg diffraction of  $\vec{P}'_3$  ( $\vec{P}'_1$ ) from the grating produced by the interference of two others.

# 10.10. Reducing light speed

L.V. Hau, Nature 397, 594 (1999).

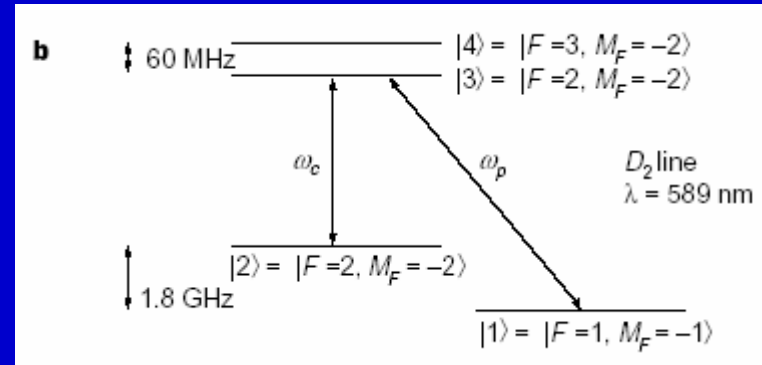
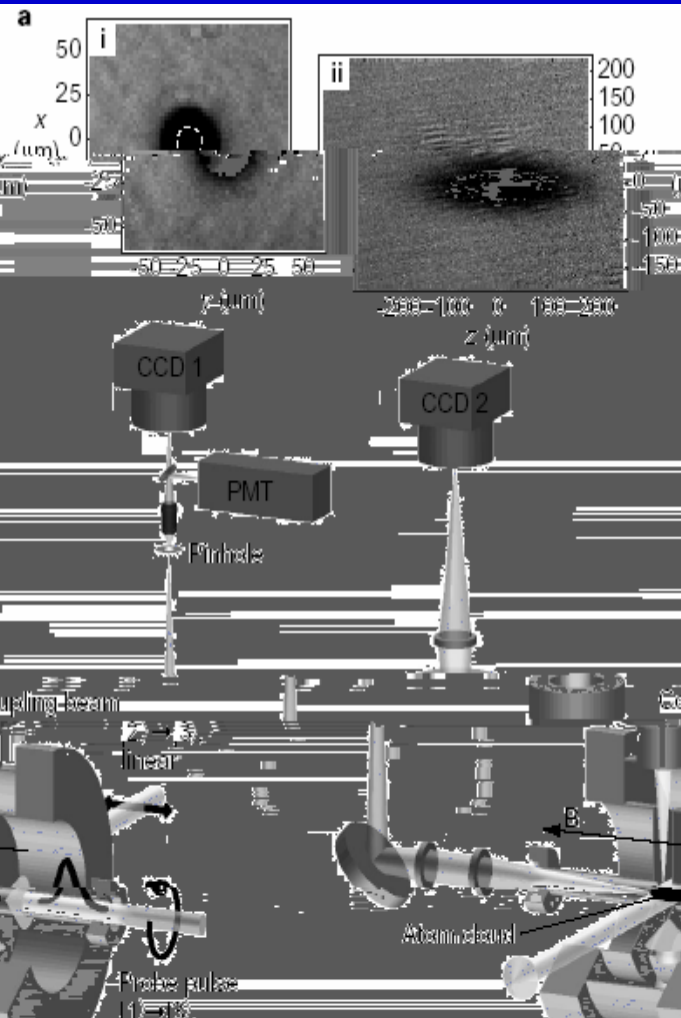


Figure 4 Experimental setup. **a**, Interference patterns observed in the absorption cell. **b**, Energy level diagram and frequency scheme.

# 10.11. Superradiance

S. Inouye et al., Science 285, 571 (1999).

**Fig. 1.** Observation of superradiant Rayleigh scattering. (A) An elongated condensate is illuminated with a single off-resonant laser beam. Collective scattering leads to photons scattered predominantly along the axial direction and atoms at 45°. (B to G) Absorption images after 20-ms time of flight show the atomic momentum distribution after their exposure to a laser pulse of a sensible duration. When the polarization was parallel to the long axis, superradiance was suppressed, and normal Rayleigh scattering was observed (B to D). For perpendicular polarization, directional, superradiant scattering of atoms was observed (E to G), and evolved to repeated scattering for longer laser pulses (F and G). The pulse durations were 25 (B), 100

(C), and 130, 350, 1100, and 1000  $\mu$ J. At the field of view of each image is 2.5 mm by 3.5 mm. The scattering angle appears larger than 45° because of the angle of observation. All images use the same color scale, except from (D) to (G), which have been scaled to match the color bar of (A).

0% 100%  
Absorption  
  
**A**  
Light  
Laser beam  
Atoms

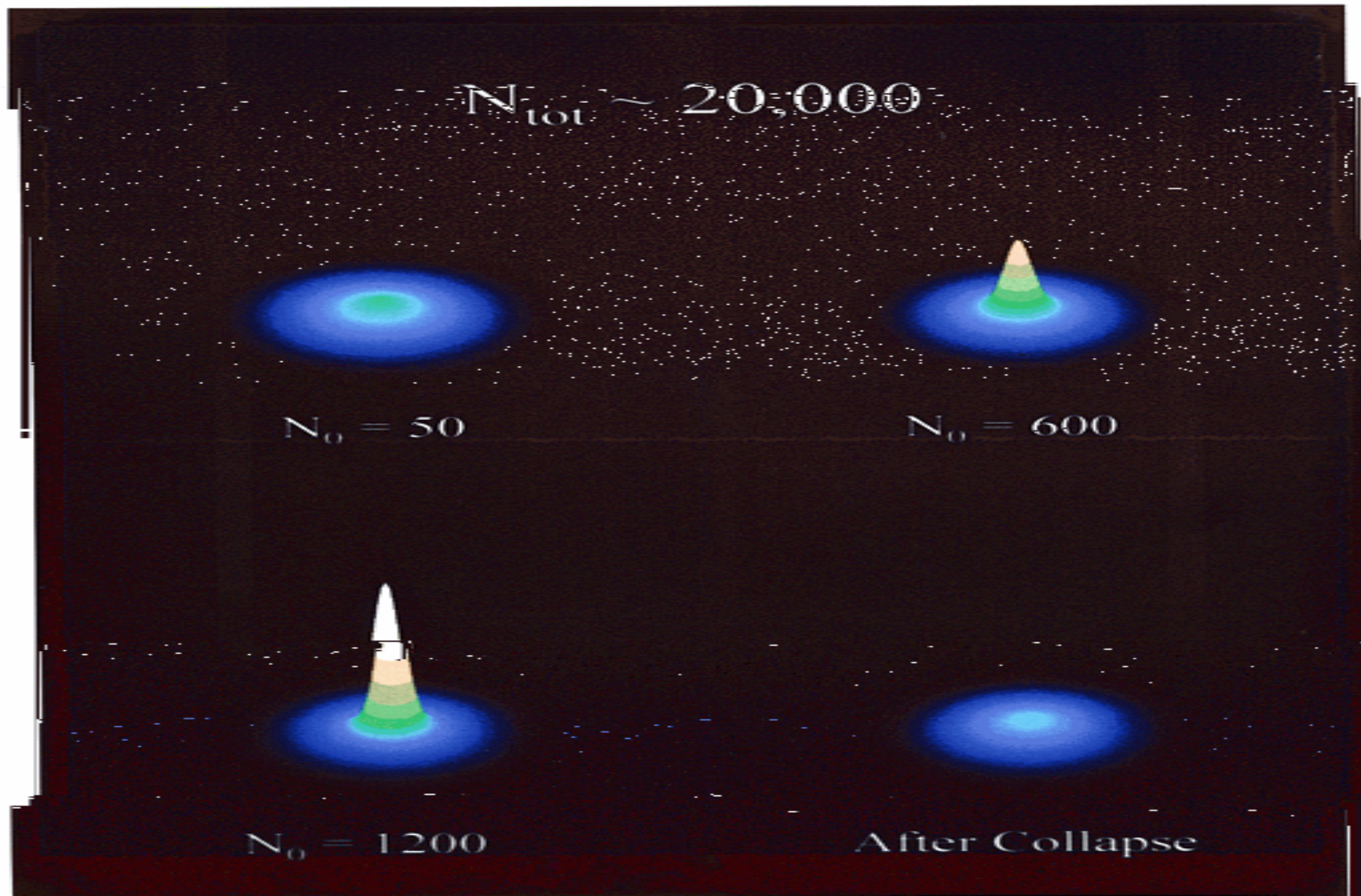
**B** **C** **D**  
**E** **F** **G**

0% 100%  
Absorption  
  
**A**  
Light  
Laser beam  
Atoms

**B** **C** **D**  
**E** **F** **G**

# 10.12. Supernova

S.L. Cornish et al., Phys. Rev. Lett. 85, 1795 (2000).

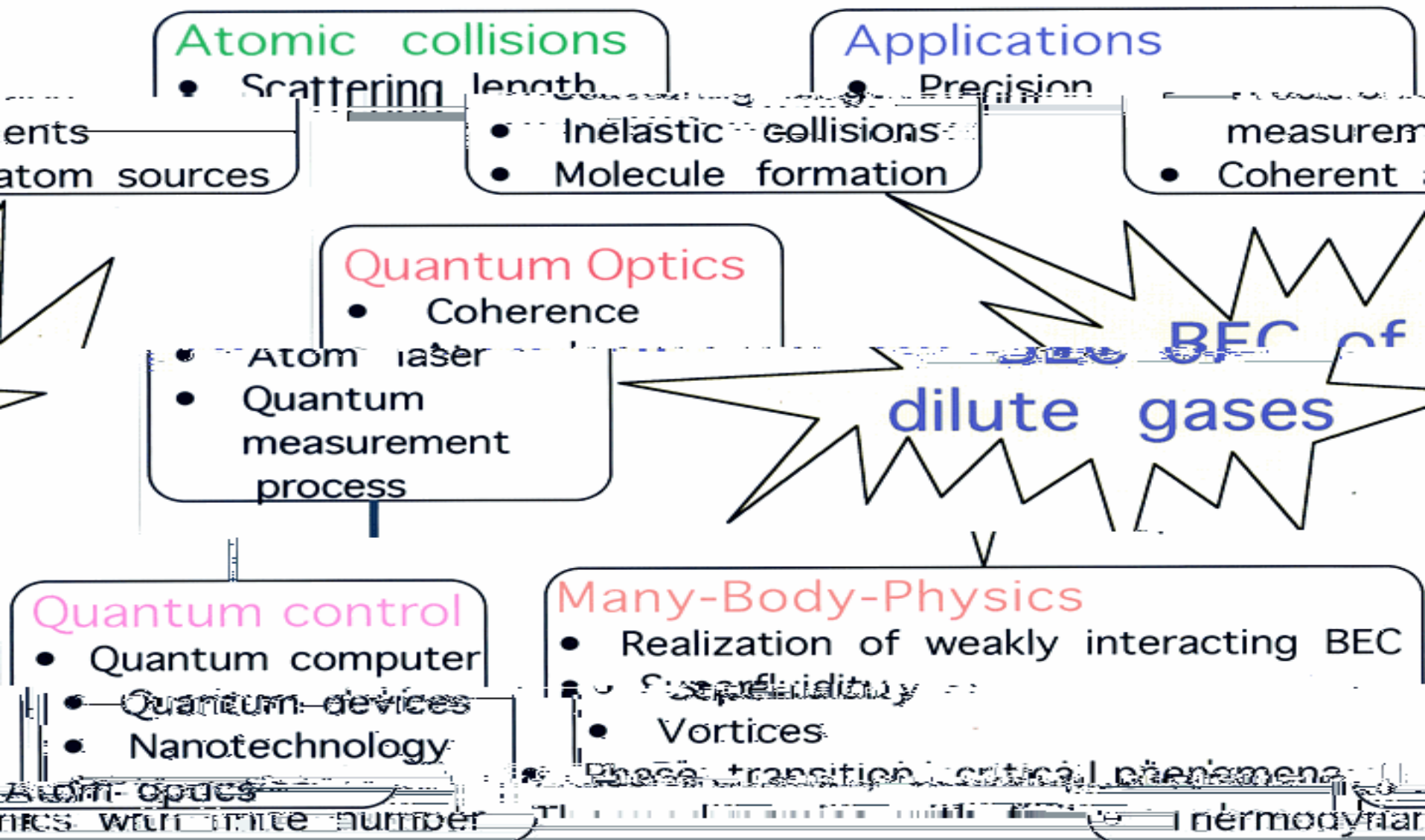


# 11. Outlook

11.1. Importance and applications

11.2. Future topics

# 11.1. Importance and applications



# 11.2. Future topics

W. Ketterle, Nature 416, 211 (2002)

' Bose-Einstein condensates become an  
ultralow-temperature laboratory  
for atom optics, collisional physics and many-  
body physics, superfluidity, quantized vortices,  
Josephson junctions and quantum phase transitions.

